

(Visualizing) Plausible Treatment Effect Paths

Simon Freyaldenhoven

Federal Reserve Bank of Philadelphia

Christian Hansen

*University of Chicago**

June 12, 2025

Abstract

We consider point estimation and inference for the treatment effect path of a policy. Examples include dynamic treatment effects in microeconomics, impulse response functions in macroeconomics, and event study paths in finance. We present two sets of plausible bounds to quantify and visualize the uncertainty associated with this object. Both plausible bounds are often substantially tighter than traditional confidence intervals, and can provide useful insights even when traditional (uniform) confidence bands appear uninformative. Our bounds can also lead to markedly different conclusions when there is significant correlation in the estimates, reflecting the fact that traditional confidence bands can be ineffective at visualizing the impact of such correlation. Our first set of bounds covers the average (or overall) effect rather than the entire treatment path. Our second set of bounds imposes data-driven smoothness restrictions on the treatment path. Post-selection Inference (Berk et al. [2013]) provides formal coverage guarantees for these bounds. The chosen restrictions also imply novel point estimates that perform well across our simulations.

JEL Codes: C12, C13

KEYWORDS: dynamic treatment effects, post-selection inference, uniform inference

*We thank Thorsten Drautzburg, Lutz Killian, Christian Leuz, Paul Mohnen, Matthew Notowidigdo, Mikkel Plagborg-Møller, Jon Roth, Jesse Shapiro, as well as audiences at the Federal Reserve Bank of Philadelphia, the University of Bonn, Georgetown University, Maastricht University, and NY Camp Econometrics for comments. The views expressed herein are those of the authors and do not necessarily reflect the views of the Federal Reserve Bank of Philadelphia or the Federal Reserve System. Emails: simon.freyaldenhoven@phil.frb.org, chansen1@chicagobooth.edu

1 Introduction

We are interested in the treatment effect path of a policy at discrete horizons $h = 1, \dots, H$. Examples include dynamic treatment effects in microeconomics, impulse response functions in macroeconomics, and event study paths in finance. We write $\beta = \{\beta_h\}_{h=1}^H$ for the vector that collects this dynamic treatment effect path up to the fixed maximum horizon of interest H . We assume access to point estimates of the parameters β_h , denoted by $\hat{\beta}_h$, that correspond to the cumulative effect of the policy at horizon $h = 1, \dots, H$. Throughout, we assume the vector that collects the estimated dynamic treatment effect path, $\hat{\beta}$, satisfies $\hat{\beta} \sim N(\beta, V_\beta)$ and that we have access to the covariance matrix V_β . Leading examples to obtain such estimates include distributed lag models, local projections, and event studies.¹ We consider both point estimation and uncertainty quantification, though our focus will be on the latter. In particular, we introduce two approaches to visualize the uncertainty about the treatment path, which we call *cumulative* and *restricted* plausible bounds. Both bounds are often substantially tighter than traditional confidence intervals, and can provide useful insights even when traditional (uniform) confidence bands appear uninformative.

The standard approach in economics to quantify and visualize the uncertainty associated with parameter estimates is to construct confidence regions. Intuitively, a confidence region visualizes to the reader what values of the parameter, in this case β , are “plausible” based on the observed data. The idea being that values inside this region appear plausible, while values outside of the region do not. The two predominant confidence regions in practice are pointwise and sup-t confidence regions (e.g. Callaway and Sant’Anna [2021]; Jordà [2023]; Boxell et al. [2024]). A third alternative is the Wald confidence region CR^{Wald} . This region simply collects all parameter values b that are not rejected by a standard Wald test of the null hypothesis that $\beta = b$ at level α . While a confidence region constructed from pointwise confidence intervals does not achieve correct coverage for the vector β , both sup-t and Wald confidence regions achieve valid coverage: $\mathbb{P}(\beta \in CR^{Wald}) = \mathbb{P}(\beta \in CR^{sup-t}) = (1 - \alpha)$.²

Sup-t and Wald confidence regions both come with some advantages and disadvantages. Since the Wald region is an ellipsoid, a disadvantage of the Wald confidence region is that

¹We abstract away from approximation issues, but note that standard asymptotic approximations within these settings along with access to consistent asymptotic variance estimators motivate this setup.

²We discuss these regions, and their construction, in more detail in Appendix A. For further discussion of uniform confidence bands, and, in particular, the merits of sup-t confidence bands, also see Freyberger and Rai [2018] and Olea and Plagborg-Møller [2019].

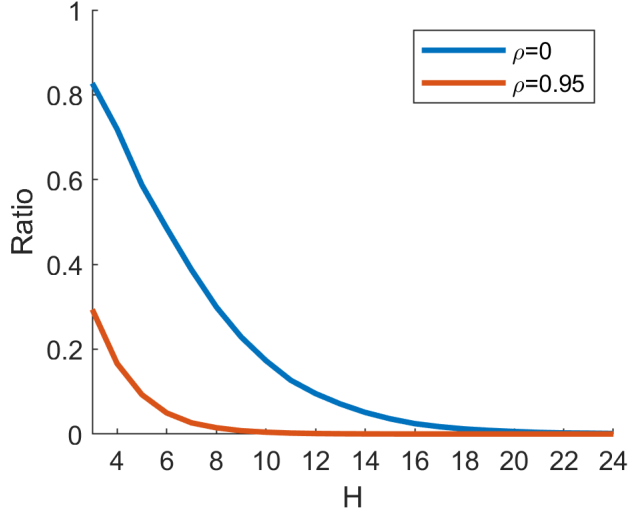


Figure 1: Volume of Wald confidence region relative to sup-t confidence region as a function of $H = \dim(\beta)$. V_β is a symmetric Toeplitz matrix with entries $v_{ij} = \rho^{|i-j|}$.

it becomes infeasible to visualize in higher dimensions (i.e. when $H > 3$). The sup-t confidence region has the advantage of being easy to visualize. However, the volume of the sup-t confidence region quickly explodes relative to the volume of the Wald region. We illustrate this difference in confidence region volume in Figure 1, which plots the volume of the Wald confidence region relative to the volume of the sup-t confidence region as a function of the dimension H for two exemplary covariance matrices V_β . We see that the volume of the sup-t region tends to be orders of magnitude larger than the volume of the Wald region for the typical horizon that is depicted in event studies and impulse responses.³ When V_β is the identity matrix ($\rho = 0$), the relative volume of the Wald region is less than 10% and around 0.1% of the volume of the sup-t region for $H = 12$ and $H = 24$ respectively. These numbers are generally even smaller if the entries in $\hat{\beta}$ have non-zero correlation: When V_β is a symmetric Toeplitz matrix with entries $v_{ij} = 0.95^{|i-j|}$, this ratio drops to 3.5% and 0.0001% for $H = 12$ and $H = 24$ respectively. One immediate consequence is that, for even moderate horizons H , the overwhelming majority of paths inside the sup-t bands would be rejected by a simple joint hypothesis test. This property seems unappealing to us and serves as a first indication that sup-t confidence bands may not always be appropriate for visualizing what dynamic treatment effect paths are plausible.

To illustrate this further, Figure 2 depicts two exemplary treatment effect plots. The object of interest is the treatment path of a policy over the depicted horizon. We have access

³In what follows, we refer to the visualizations of $\hat{\beta}$ simply as treatment effect plots.

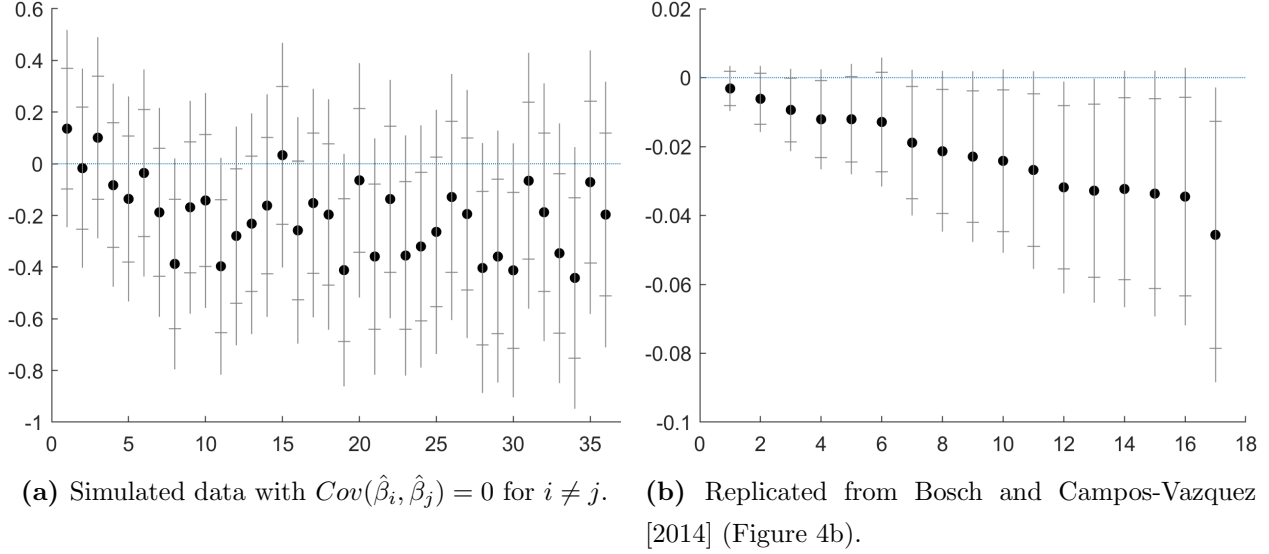


Figure 2: Two exemplary treatment effect plots, including point estimates, and pointwise and sup-t confidence intervals.

to jointly normal estimates $\{\hat{\beta}_h\}_{h=1}^H$, with observed point estimates $\hat{\beta}$ given by the black dots. Both panels further include pointwise 95 percent confidence intervals (inner confidence set as indicated by the dashes) and uniform 95 percent sup-t confidence bands (outer confidence set). While the pointwise confidence intervals only permit testing of pre-selected hypotheses for individual coefficients β_h , the sup-t bands contain the entire true path β in 95 percent of realized samples. Figure 2a depicts a hypothetical example with zero correlation between the estimated coefficients.⁴ Figure 2b is based on the same estimates as Figure 4b in Bosch and Campos-Vazquez [2014]. In this example, all off-diagonal entries in V_β are positive, and the average correlation between adjacent coefficients is 0.95.

The sup-t region in Figure 2a includes treatment paths that imply an overall positive effect (paths with $\sum_{h=1}^H \beta_h > 0$) and treatment paths with very different shapes. In fact, $\beta = 0$ falls inside the sup-t bands, suggesting that the null of “no treatment effect” is plausible. However, a joint test of the null hypothesis that $\beta = 0$ yields a p-value of 1.54×10^{-9} . In contrast, $\beta = 0$ falls outside the sup-t bands in Figure 2b, suggesting that the null of “no treatment effect” is not plausible. However, a joint test of the null hypothesis that $\beta = 0$ yields a p-value of 0.33. These discrepancies between the easy-to-visualize sup-t region and the results of simple joint hypothesis tests again suggest to us that the sup-t confidence region may not always be providing an empirically effective visualization of what treatment

⁴We give more detail on the underlying DGP in Section 4.

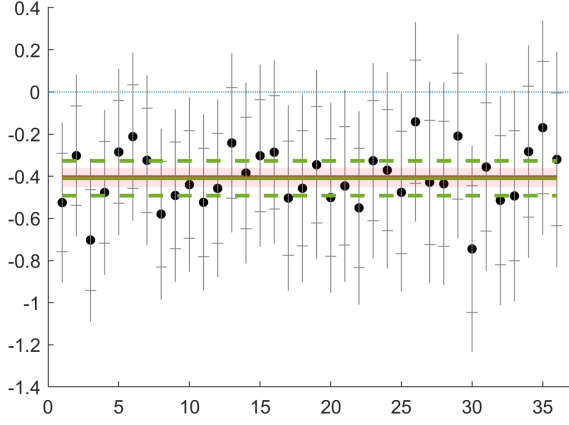
effect paths are plausible.

In Figure 3, we therefore introduce two alternative ways to visualize plausible treatment effect paths. Panels 3a-3d are based on different simulated data generating processes, while panels 3e and 3f are based on published figures in Macroeconomics (Nakamura and Steinsson [2018]) and Applied Micro (Bosch and Campos-Vazquez [2014]). Elements from the “standard” treatment effect plot are provided by the black dots which give point estimates of the treatment effect at each horizon and by the inner and outer confidence intervals corresponding respectively to the usual pointwise and sup-t confidence intervals.⁵ In addition, panels 3a-3d include a solid blue line to represent the true treatment effect path and an additional dotted red line, which we explain below. Finally, each plot includes two new features: (i) the shaded red area, and (ii) the dashed and solid green lines. Importantly, these new features shift the goal posts relative to the Wald and sup-t bounds, and the inferential target of our bounds is *not* the true treatment path.

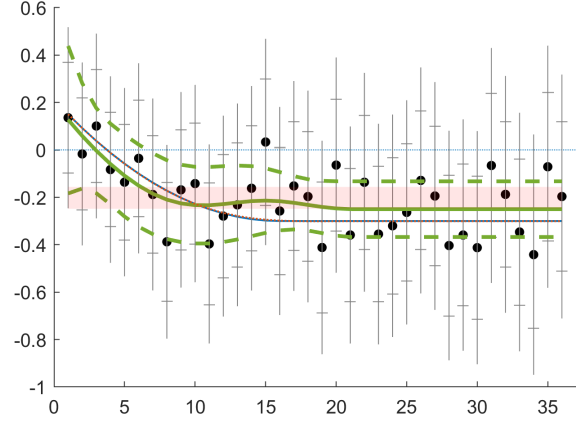
The shaded red area represents our proposed 95% *cumulative plausible bounds*. We construct these bounds so that the average treatment effect across the depicted horizons will be within these bounds for 95% of all realizations of the data. For example, in Figure 3b, these bounds suggest that the average effect of the policy over the 36 periods depicted is between $(-0.248, -0.156)$, and thus that the overall effect of the policy over the 36 periods is strictly negative and inside the window $(-8.93, -5.62)$. In contrast to the standard sup-t region, these bounds suggest that a treatment path with no overall effect of the policy is not plausible. These cumulative plausible bounds have an alternative interpretation in terms of the overall treatment effect path. Specifically, the cumulative plausible bounds are such that the treatment path β (depicted as the solid blue line) will *on average* be within these bounds for 95% of all realizations of the data.

The dashed green lines represent our proposed 95% *restricted plausible bounds*, which are centered around *restricted estimates* provided by the solid green line. These restricted estimates and bounds are motivated by envisioning a researcher who is interested in understanding key features of the treatment effect path but is not concerned with necessarily covering the entire true path at every horizon. However, we also imagine the researcher as being *ex ante* unsure about what the important features are and wanting to use the data to help select a restricted model for summarizing the treatment effect path.

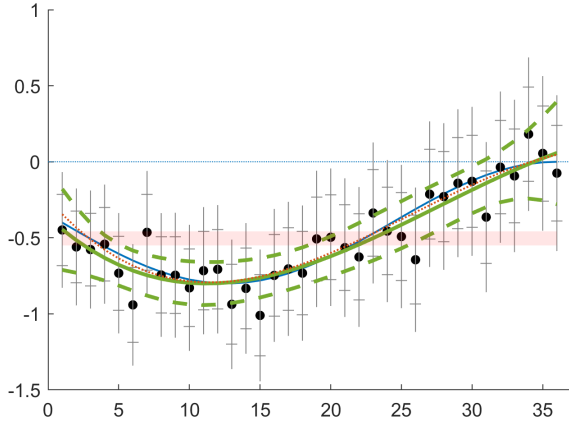
⁵Figure 3b is based on the same estimates $\hat{\beta}$ as Figure 2a. Figure 3f is based on the same estimates $\hat{\beta}$ as Figure 2b.



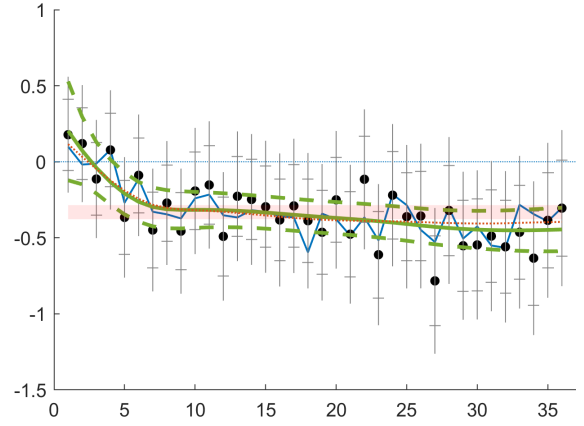
(a) treatment path constant



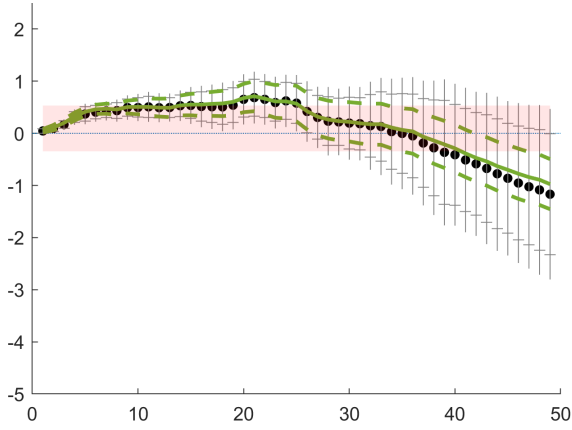
(b) treatment path smooth, eventually flat



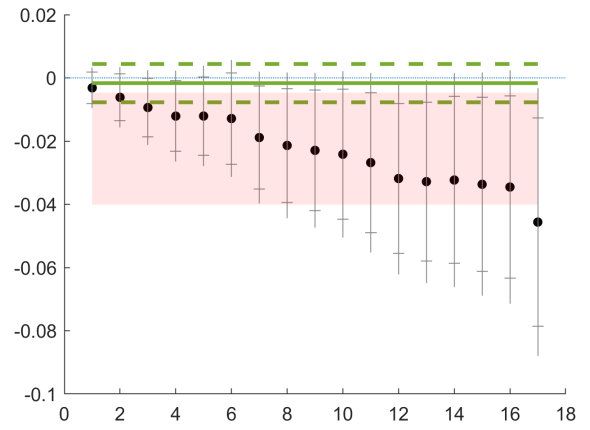
(c) treatment path hump-shaped



(d) treatment path wiggly



(e) Replicated from Nakamura and Steinsson [2018] (Figure A.2)



(f) Replicated from Bosch and Campos-Vazquez [2014] (Figure 4b)

Figure 3: Exemplary treatment effect plots including our proposals. Our proposed visualization includes two additional objects. The shaded red areas provides the *cumulative plausible bounds*. The dashed green lines provide the *restricted plausible bounds*, and the thick solid green line provides the corresponding restricted estimates. In the simulated panels a)-d), we further include the true treatment path (thin blue line) and its *surrogate* (dotted red line).

More concretely, we construct the restricted estimates and plausible bounds by using a statistical model selection procedure to select an approximating model from within a pre-specified universe of candidates. We consider a default set of models motivated by a preference for smooth dynamics that eventually die out induced by shrinking first and third differences of $\hat{\beta}$, though we note that the procedure could be applied with any finite, pre-specified universe of models. The restricted estimates are then simply the point estimates of the treatment path based on the selected model. We construct the restricted plausible bounds to provide uniform (95%) coverage accounting for data-dependent model selection by applying Berk et al.’s [2013] Post-Selection Inference (PoSI) to our setting.

Looking at the restricted estimates and restricted plausible bounds in each panel paints a starkly different picture compared to the sup-t intervals. In all cases, the restricted plausible bounds are relatively narrow and seemingly quite informative about the broad features of the treatment effect paths. Figure 3f stands out and merits further discussion. In this instance, our model selection procedure selects a constant treatment effects model. Our restricted estimates then coincide with the MLE estimate of a constant treatment effects model.⁶ Remarkably, this estimate is -0.0017 , which is outside of the convex hull of the individual estimates $\hat{\beta}_h$.⁷ Further, a Wald test of the null hypothesis that $\beta_h = -0.0017$ for $h = 1, \dots, H$ gives a p-value of 0.36. That is, a traditional joint hypothesis test suggests there is relatively little evidence against this hypothesis, which thus appears relatively “plausible,” contrary to what a visual inspection of the traditional treatment effect plot might suggest. This difference underscores that traditional treatment effect plots may be ineffective at visualizing the impact of the off-diagonal entries in V_β (we illustrate this further in Appendix A). In contrast, the entire covariance matrix V_β is reflected in our restricted plausible bounds. Accounting for the covariance structure can lead to interestingly different results, improving the informativeness of these plots.

Finally, we reiterate that the inferential target of the restricted plausible bounds in the population is *not* the true treatment path. Rather, the restricted plausible bounds provide uniform coverage of a *surrogate* path given by the approximation that would be obtained by applying the selected model to the true effect path. We depict the selected surrogate for each of the simulated scenarios in Figure 3 with a dotted red line. In Figure 3a and Figure

⁶That is, a model with $\hat{\beta} \sim N(\beta, V_\beta)$, where β is constant across h .

⁷Intuitively, this behavior results from the strong positive correlation in the estimates combined with more precise estimates in early periods. We note that this strong positive correlation in the estimates cannot be inferred from the traditional plot.

3b, this surrogate is indistinguishable from the true treatment path. In Figure 3c and Figure 3d, the surrogate differs from the true treatment path but visually captures what seem to be key features of the overall treatment path. Indeed, we suspect many empirical researchers, if given the true treatment path from Figure 3d, would actually be more interested in the smooth approximation provided by the surrogate in this case. That is, we view the fact that the restricted plausible bounds cover a data-dependent approximation to the population treatment effect path as a potentially appealing feature.

In summary, we propose augmenting standard event-study plots with two additional elements: a shaded red region (the cumulative plausible bounds) and dashed and solid green lines (the restricted plausible bounds and estimates, respectively). Together with the usual pointwise and sup-t intervals, these visualizations offer a more comprehensive view of plausible effect paths, each serving distinct inferential purposes. Sup-t bands provide a simple, assumption-free summary of plausible paths. Pointwise intervals target effects at specific horizons. Cumulative bounds inform average treatment effects, while restricted bounds and estimates capture approximations of the effect path obtained using data-driven smoothing.

Our paper connects to several strands in the literature. We obtain our restricted plausible bounds and estimates by considering a finite set of candidate models for β . This approach is thus closely related to work that considers parametric models and approximations to β . Such approaches have been studied going back at least to Almon [1965], who imposes a parametric model on distributed lag coefficients. More recently, Barnichon and Matthes [2018] propose approximating impulse responses with a set of basis functions, and Barnichon and Brownlees [2019] propose to shrink impulse response estimates towards polynomials. While related, we differ from these approaches by focusing on inference for a data-dependent surrogate effect path; see, for example, Genovese and Wasserman [2008] for a general discussion of inference on surrogates.

We operationalize our restricted plausible bounds by using data-dependent selection from a universe of candidate models with different fixed degrees of shrinkage over first and third differences. This model universe is closely related to the structure employed in Shiller [1973] which takes a fully Bayesian approach to estimating a distributed lag model under a normal prior on the d^{th} order difference of β . Our restricted estimates are thus akin to point estimates that could be obtained by taking an empirical Bayes approach within the framework of Shiller [1973]. From the empirical Bayes perspective, one could then potentially adapt

Armstrong et al. [2022] to the present context to obtain interval estimates.⁸ In contrast, our restricted plausible bounds provide frequentist coverage for the population value of the selected surrogate path.

To maintain coverage guarantees for the selected surrogate, accounting for data dependent model selection, we use a version of post-selection inference (PoSI) confidence intervals (Berk et al. [2013]). Given that our inferential target is the population value of the selected model, we note that one could adopt other approaches from the literature on selective inference; see, e.g., Taylor and Tibshirani [2015] and Kuchibhotla et al. [2022] for excellent reviews.

There are a variety of other approaches to quantifying and visualizing uncertainty about treatment effect paths available in the literature. For example, Sims and Zha [1999] argues that conventional pointwise bands common in the literature should be supplemented with measures of shape uncertainty, and proposes such measures. Jordà [2009] suggests a method to construct simultaneous confidence regions for impulse responses given propagation trajectories. Freyberger and Reeves [2018] propose a uniformly valid inference method for an unknown function or parameter vector satisfying certain shape restrictions. More generally, inference for the treatment effect path is tightly tied to more general nonparametric inference problems; see, e.g., Chen et al. [forthcoming] for an interesting recent example that explicitly allows for use of a data-dependent sieve dimension. The “shotgun plot” of Inoue and Kilian [2016], which depicts a random sample of B impulse responses contained in the joint Wald confidence set, provides an alternative approach to visualizing plausible treatment effect paths. We believe our proposal to provide simple additional visual elements to the usual treatment effect plot provides a useful complement to this existing literature.

2 Cumulative Plausible Bounds

We first present a simple visual feature, the *cumulative plausible bounds*, that can be added to a standard treatment effect plot. This visualization does not impose any functional form or smoothness assumptions on the underlying treatment path, but, in terms of the full treatment effect path, it also does not achieve uniform coverage. Rather, the cumulative plausible bounds use a weaker notion of “cumulative coverage”: The true treatment path will *on average* be within the cumulative plausible bounds in $(1 - \alpha)\%$ of all realizations of

⁸Also see the SmIRF estimator of Plagborg-Møller [2016] for a related approach that includes confidence sets with guaranteed frequentist coverage.

the data for a given significance level α . That is, by providing valid inference for the average effect over the horizon H , our cumulative plausible bounds provide a simple visual element that conveys uncertainty about the average treatment effect.

These cumulative plausible bounds are simply visualizations of the dynamic treatment path corresponding to the largest and smallest sum of all treatment effects up to horizon H not rejected by a standard hypothesis test. They can be interpreted as boundary paths that would be consistent with the upper and lower limits of a confidence interval for the overall effect of the policy over H periods. Formally, let

$$u^{1-\alpha} = \max \sum_{h=1}^H \beta_h^* \quad \text{s.t. } (\beta^* - \hat{\beta})' V_{\beta}^{-1} (\beta^* - \hat{\beta}) = \kappa^{(1-\alpha)}, \quad (1)$$

where $\kappa^{(1-\alpha)}$ denotes the inverse of the chi-square cdf with one degree of freedom at chosen significance level $(1 - \alpha)$. We further define $l^{1-\alpha}$ analogously, replacing the max in (1) with min. Since both $u^{1-\alpha}$ and $l^{1-\alpha}$, corresponding to the upper and lower limit of the overall effect are scalars, there are infinitely many treatment paths that correspond to these bounds on the overall treatment effect. To visualize the bounds, we use $(U, L)^{1-\alpha} = \{U_h^{1-\alpha}, L_h^{1-\alpha}\}_{h=1}^H$, where $U_h^{1-\alpha} = \frac{u^{1-\alpha}}{H}$ and $L_h^{1-\alpha} = \frac{l^{1-\alpha}}{H}$.⁹ We choose this visualization as the interval $(U, L)^{1-\alpha}$ is a $(1 - \alpha)\%$ Wald confidence interval for the average effect of the policy over the horizon H , $\frac{1}{H} \sum_{h=1}^H \beta_h$.

The following trivial proposition clarifies how coverage of these cumulative plausible bounds relates to coverage of the treatment path.

Proposition 1. *The true treatment path β will on average (over H) be within the cumulative plausible bounds for $(1 - \alpha)$ of all realizations:*

$$\mathbb{P} \left(\frac{\sum_{h=1}^H L_h^{1-\alpha}}{H} < \frac{\sum_{h=1}^H \beta_h}{H} < \frac{\sum_{h=1}^H U_h^{1-\alpha}}{H} \right) = (1 - \alpha). \quad (2)$$

Proof. By construction, a Wald test on the cumulative treatment effect with significance level $(1 - \alpha)$ will reject

- a) any treatment path $\tilde{\beta}_h$ with $\sum_{h=1}^H \tilde{\beta}_h > \sum_{h=1}^H U_h^{1-\alpha}$,
- b) any treatment path $\tilde{\beta}_h$ with $\sum_{h=1}^H \tilde{\beta}_h < \sum_{h=1}^H L_h^{1-\alpha}$.

⁹Instead of using bounds $(U, L)^{1-\alpha}$ that are constant across h , one could alternatively depict bounds that reflect the shape of the unrestricted estimates.

Since a Wald test for the cumulative effect has correct size, the result follows immediately. \square

Proposition 1 states that, for a given significance level α , the true treatment path will *on average* be within our bounds for $(1 - \alpha)\%$ of all realizations. This follows immediately from the fact that any path that is not, on average, inside the cumulative plausible bounds implies an overall treatment effect over H periods that is rejected by the corresponding hypothesis test.

3 Restricted Plausible Bounds

The second idea we pursue is to present confidence regions that cover approximations of the true effect path that have “reasonable shapes.” We term these confidence regions *restricted plausible bounds*. Here, we define “reasonable shapes” by pre-specifying a universe of models. We then use data-dependent model selection to choose a good representation for $\hat{\beta}$ from among this set. Intuitively, this approach is related to directly imposing a functional form restriction as is often done in empirical work, for example by

- specifying a parametric model for β , e.g. imposing a constant treatment effects model ($\beta_h = \beta_{h'} \forall h, h'$),
- aggregating the underlying dataset over time (e.g. monthly to quarterly), which effectively restricts β to “step functions,”
- estimating an impulse response function (IRF) via a vector auto regression (VAR), which restricts the IRF to functional forms compatible with the chosen VAR (cf. the discussions in Li et al. [2024] and Olea et al. [2024]).

One key feature of our approach is that we do not rely on a fixed functional form restriction or make use of some other implicit or ad hoc device to choose a restricted model. Rather, we select a model, and then take model selection explicitly into account when constructing confidence bounds. That is, we propose a model selection procedure that is explicit, transparent, and will allow us to maintain formal coverage guarantees instead of implicitly using the data to select a restricted model, which leads to invalid inference.

Before we formally define our proposal, we introduce some necessary notation. We first borrow from the nonparametric statistics literature to introduce the notion of a “surrogate”

(cf. Genovese and Wasserman [2008]). A surrogate path β_M is close to, but potentially simpler than, β . We note that the surrogate path is a population object that approximates β , the true treatment path. For example, we may define a constant treatment effects surrogate of β as $\beta_s = \arg \min_b (\beta - b)'(\beta - b)$ s.t. $\Delta b = 0$. If the surrogate model M is fixed a priori (and not itself a function of the data), inference for β_M is straightforward, though we stress that any inferential statements in this case will be about β_M and not β .¹⁰ However, failing to take into account that the data is used to select the surrogate creates a problem for inference (e.g. Leeb and Pötscher [2005] or Roth [2022]). In our setting the surrogate is explicitly a function of the data (or more precisely, of the unrestricted estimates $\hat{\beta}$), and we may thus write $\beta_{M(\hat{\beta})}$ to denote a data dependent surrogate path. In a first step, we use the data to select the surrogate model. In a second step, we then create a uniformly valid confidence region for the selected surrogate path, taking into account that the choice of surrogate is also random (i.e. a function of the data).

Given that we are doing model selection from a specified universe of models, a key choice is the specific model universe we consider. We consider a model universe motivated by the following economic intuition:

1. The dynamics of the treatment effect die off eventually. That is, after K periods, the treatment effect is constant. We treat K as unknown and allow K to be as large as H , thus allowing dynamics across the entire depicted horizon.
2. The dynamic treatment path is “smooth,” where we measure smoothness using the third differences of the treatment path.

In practice, we use shrinkage over first and third differences of $\hat{\beta}$ to implement 1. and 2.

Formally, we assume that the estimates of the treatment path $\hat{\beta}$ are jointly normal with $\hat{\beta} \sim N(\beta, V_\beta)$, where $V_\beta = \sigma^2 V$, $\sigma^2 = \frac{1}{H} \sum_{h=1}^H V_\beta(h, h)$, and V is positive-definite. Taking $\hat{\beta}$ as input, we define the following object:

$$\begin{aligned} \tilde{\beta}(\lambda_1, \lambda_2, K) &= \arg \min_b Q(b, \lambda_1, \lambda_2, K) \\ &= \arg \min_b \underbrace{(\hat{\beta} - b)' V^{-1} (\hat{\beta} - b)}_{\text{distance from } \hat{\beta}} + \lambda_1 \underbrace{b' D_1' W_1(K) D_1 b}_{\text{penalty on first difference after horizon } K} + \lambda_2 \underbrace{b' D_3' W_3 D_3 b}_{\text{penalty on third difference}} \end{aligned} \quad (3)$$

¹⁰Targeting a simple surrogate function is akin to the standard approach in economics of estimating linear models even when the conditional expectation function is not believed to be linear. One can think of the linear model as a “surrogate model” capturing the best linear predictor. Inference will then be about the linear surrogate, and not the “truth.”

where

- D_1 and D_3 are the $(H \times H - 1)$ and $(H \times H - 3)$ first and third difference operators,
- $\eta = (\lambda_1, \lambda_2, K)$ are tuning parameters,
- $W_1(K)$ and W_3 are weighting matrices where $W_1(K)$ only places weight on first differences for horizon $K \leq H$ and beyond (See Appendix B for further details.).

Solving (3) provides a closed form solution¹¹ for $\tilde{\beta}(\lambda_1, \lambda_2, K) := \tilde{\beta}(M)$ given by

$$\begin{aligned}\tilde{\beta}(M) &= (V^{-1} + \lambda_1 D_1' W_1(K) D_1 + \lambda_2 D_3' W_3 D_3)^{-1} V^{-1} \hat{\beta} \\ &= P(M) \hat{\beta}.\end{aligned}$$

For fixed $M = (\lambda_1, \lambda_2, K)$, it immediately follows that

$$\tilde{\beta}(M) - P(M)\beta \sim N(0, V_M), \quad (4)$$

where $V_M = P(M)V_\beta P(M)'$. Here, $P(M)\beta = \beta_M$ defines a particular surrogate path for β . Intuitively, $P(M)\beta$ corresponds to a “projection” of the true treatment path β into a lower dimensional space. Given (4), it would be straightforward to construct a confidence region for $\{\beta_{M,h}\}_{h=1}^H$, where $\beta_{M,h}$ denotes the h^{th} entry in vector β_M , for a given, fixed value of the tuning parameters. However, knowing *ex ante* what values to use for λ_1 , λ_2 , and K seems challenging. We thus use model selection to choose λ_1 , λ_2 , and K — or, equivalently, to choose the surrogate model M .

Specifically, we use the estimated $\hat{\beta}$ and an object akin to an information criterion to select the surrogate M . First, note that we can construct the “residuals” $\hat{\beta} - \tilde{\beta}(M) = \hat{\beta} - P(M)\hat{\beta} = (I - P(M))\hat{\beta}$. We use this residual formulation to define an analog of model

¹¹For intuition, note that the problem in (3) is closely related to the following constrained optimization with tuning parameters c_1 , c_2 , and K , explicitly bounding the first and third difference:

$$\begin{aligned}\hat{\beta}(c_1, c_2, K) &= \arg \min_b \underbrace{(\hat{\beta} - b)' V^{-1} (\hat{\beta} - b)}_{\text{distance from } \hat{\beta}} \\ \text{such that } &\underbrace{b' D_1' W_1(K) D_1 b}_{\text{small first difference, after horizon } K} \leq c_1 \quad \text{and} \quad \underbrace{b' D_3' W_3 D_3 b}_{\text{small third difference}} \leq c_2.\end{aligned}$$

However, this formulation does not have a closed form solution and is computationally more challenging, making it less appealing in practice.

degrees of freedom given by $\text{df}(M) = \text{trace}(P(M))$. We then select a model that minimizes a BIC analog over \mathcal{M} where \mathcal{M} denotes the universe of values for $M = (\lambda_1, \lambda_2, K)$:

$$\hat{M} = \arg \min_{M \in \mathcal{M}} (\hat{\beta} - \tilde{\beta}(M))' V_{\tilde{\beta}}^{-1} (\hat{\beta} - \tilde{\beta}(M)) + \log(H) \text{df}(M).$$

We tie the researcher’s hands by pre-specifying \mathcal{M} , the universe of models considered. In our implementation, \mathcal{M} includes surrogate models corresponding to a constant, linear, quadratic and cubic treatment effect path (with one, two, three, and four degrees of freedom respectively), as well as an unrestricted model corresponding to the unrestricted estimates $\hat{\beta}$ (with H degrees of freedom). \mathcal{M} further includes surrogate models corresponding to surrogate paths of the form $P(M)\beta = \beta_M$ using a grid over $(\lambda_1, \lambda_2, K)$. We discuss our implementation in more detail in Appendix B and visualize the model universe \mathcal{M} for four exemplary treatment paths β in Online Appendix Figure 12, but note that \mathcal{M} does not depend on $\hat{\beta}$ or σ .

Remark 1. *One could use other model universes and shrinkage methods. Examples of alternative approaches include Barnichon and Matthes [2018] and Barnichon and Brownlees [2019]. We have chosen a class that we believe will be a reasonable representation of beliefs in many applications. Our approach with this model class is also particularly easy computationally, which allows us to nest a large universe of models. Likewise, one could select the surrogate model M using methods other than minimizing our BIC analog. We found that the specific structure and estimation we employ performed well across our simulations and believe it provides a good default.*

Given the selected surrogate \hat{M} , we define the *restricted estimates* as $\tilde{\beta}(\hat{M})$. However, we cannot directly apply (4) to obtain a valid confidence region for the population value of the surrogate path $\beta_{\hat{M}} = P(\hat{M})\beta$ because \hat{M} was selected by looking at the data, $\hat{\beta}$. Thus, in a second step, we use Valid Post-Selection Inference (Berk et al. [2013]), which explicitly accounts for data-dependent (and thus random) model selection, to construct a uniformly valid confidence region for $\beta_{\hat{M}}$. These confidence intervals, our *restricted plausible bounds*, are rectangular regions of the form $CR^{POSI} = \{\ell_h(X), u_h(X)\}_{h=1}^H$ for $[\ell_h(X), u_h(X)] = [\tilde{\beta}(\hat{M})_h \pm C^\alpha V_{\hat{M}}^{1/2}(h, h)]$ where $\tilde{\beta}(\hat{M})_h$ denotes the restricted estimate of the effect at horizon h and $V_{\hat{M}}^{1/2}(h, h)$ is the square root of the h^{th} diagonal entry of $V_{\hat{M}}$. To ensure uniform validity we use the “PoSI constant” of Berk et al. [2013] as C^α , defined as the minimal value that satisfies

$$\mathbb{P} \left(\max_{M \in \mathcal{M}} \max_h |t_{h,M}| \leq C^\alpha \right) \geq (1 - \alpha),$$

where $t_{h \cdot M} = V_M^{-1/2}(h, h)\xi_h$, and ξ_h is the h^{th} element of multivariate normal vector ξ with mean $\mathbf{0}_H$ and variance V_M . Importantly, C^α depends on \mathcal{M} , the universe of models considered, but not on the model selection procedure.

The following proposition is a direct application of Berk et al. [2013].

Proposition 2. *For any treatment path β , we obtain valid coverage for its surrogate $\beta_{\hat{M}}$:*

$$\mathbb{P}[\beta_{\hat{M}} \in CR^{POSI}] \geq 1 - \alpha. \quad (5)$$

Proof. This follows immediately from the guarantees in Berk et al. [2013]:

$$\mathbb{P}(\beta_M \in CR^{POSI} | \hat{M} = M) \geq 1 - \alpha.$$

□

Proposition 2 guarantees that our restricted plausible bounds cover the selected surrogate to the truth in at least $(1 - \alpha)\%$ of sample realizations.

Remark 2. *An immediate consequence of Proposition 2 is that $\mathbb{P}(\beta \in CR^{POSI}) \geq 1 - \alpha$ if $\mathbb{P}(\beta_{\hat{M}} = \beta_M = \beta) = 1$. That is, in cases where model selection is effectively non-random and the selected surrogate path coincides with β , the restricted plausible bounds will also provide valid coverage for the true treatment path. Given the form of our BIC type objective for selecting \hat{M} and that the unrestricted estimates are always included in our default model universe, one could provide conditions for $\mathbb{P}(\beta_{\hat{M}} = \beta_M = \beta) = 1$ under a sequence of models where $\sigma^2 \rightarrow 0$ and surrogate paths were well-separated – e.g. where $\|\beta - \beta_M\| \geq \delta > 0$ for all candidate models M such that $\beta_M \neq \beta$. While technically possible, we i) question the utility of this perspective in offering a useful finite sample approximation and ii) view the surrogate as an economically interesting summary of the treatment path in itself.*

Remark 3. *Throughout, we work with the unrestricted estimates $\hat{\beta}$. Our motivation is to augment visualizations of treatment effect paths within the setting where $\hat{\beta} \sim N(\beta, V_\beta)$ provides a reasonable approximation. We further note that the interpretation of treatment effect plots as currently displayed with point estimates and pointwise confidence intervals essentially relies on exactly this approximation. An alternative would be to estimate the restricted models directly on the data. In settings where $\hat{\beta} \sim N(\beta, V_\beta)$ provides a good approximation, we suspect that such an approach will yield qualitatively similar results. It may be interesting to explore directly estimating restricted models in settings where the approximation $\hat{\beta} \sim N(\beta, V_\beta)$ is questionable.*

4 Numerical Results

In this section, we illustrate the properties of our restricted plausible estimates and bounds as well as our cumulative plausible bounds in simulation experiments with treatment paths generated to resemble treatment path dynamics that practitioners may encounter. We illustrate these treatment paths in Figure 4. We consider a constant treatment effect path (cf. Figure 4a); a treatment path that smoothly declines before flattening out after 17 periods (cf. Figure 4b); a hump-shaped treatment path with dynamics that continue for the entire H periods (cf. Figure 4c); and a “wiggly” treatment path (cf. Figure 4d). We describe the exact DGP for each of the four panels in more detail in Online Appendix Table 1.¹² The object of interest is the treatment path over a 36-month horizon. We have access to jointly normal estimates $\{\hat{\beta}_h\}_{h=1}^{36}$. For each of these four treatment paths, we then draw 1,000 realizations of $\hat{\beta} \sim N(\beta, V_\beta)$.¹³

We first compare the point estimation properties of the unrestricted estimates $\hat{\beta}$ with our restricted estimates $\tilde{\beta}(\hat{M})$ for each of these four scenarios. In particular, Figure 5 depicts the ratio in mean-squared error, $MSE_{\tilde{\beta}(\hat{M})}/MSE_{\hat{\beta}}$, as a function of σ^2 , which scales the covariance matrix of the estimates, V_β (see Online Appendix C for more detail). The largest value of σ^2 in Figure 5 (corresponding to the left most point) thus represents relatively noisy estimates.¹⁴ We conclude that in most cases our restricted estimator has excellent point estimation properties when the target is the true treatment path β . In the three panels that have a smooth treatment path (Figures 5a-5c), the MSE of our restricted estimate is a full order of magnitude lower compared to the unrestricted estimate. In Figure 5d, our restricted estimate has a lower MSE when estimates are very noisy, a higher MSE for intermediate sizes of σ^2 , and a similar MSE when σ^2 is small. However, we suspect that a lower-dimensional summary of β , as provided by the surrogate path, may in fact be the policy relevant object in cases where the true treatment path exhibits complicated dynamics as in this panel (cf. Figure 4d).

We next turn our attention to inference and first look at coverage. We again consider the four previous DGPs and vary the amount of noise in the estimation of β by varying σ^2 . The

¹²Figure 3 provides one example realization from each of these DGPs.

¹³In the figures that follow, V_β is diagonal with its entries specified in Online Appendix C. We repeat our exercise with more general covariance matrices in Online Appendix E.

¹⁴Figure 3 was created from a single realization of the the left most point in Figure 5. To give the reader a sense of the scale of the x-axes, Online Appendix Figure 11 also illustrates a single realization of the right most point in Figure 5.

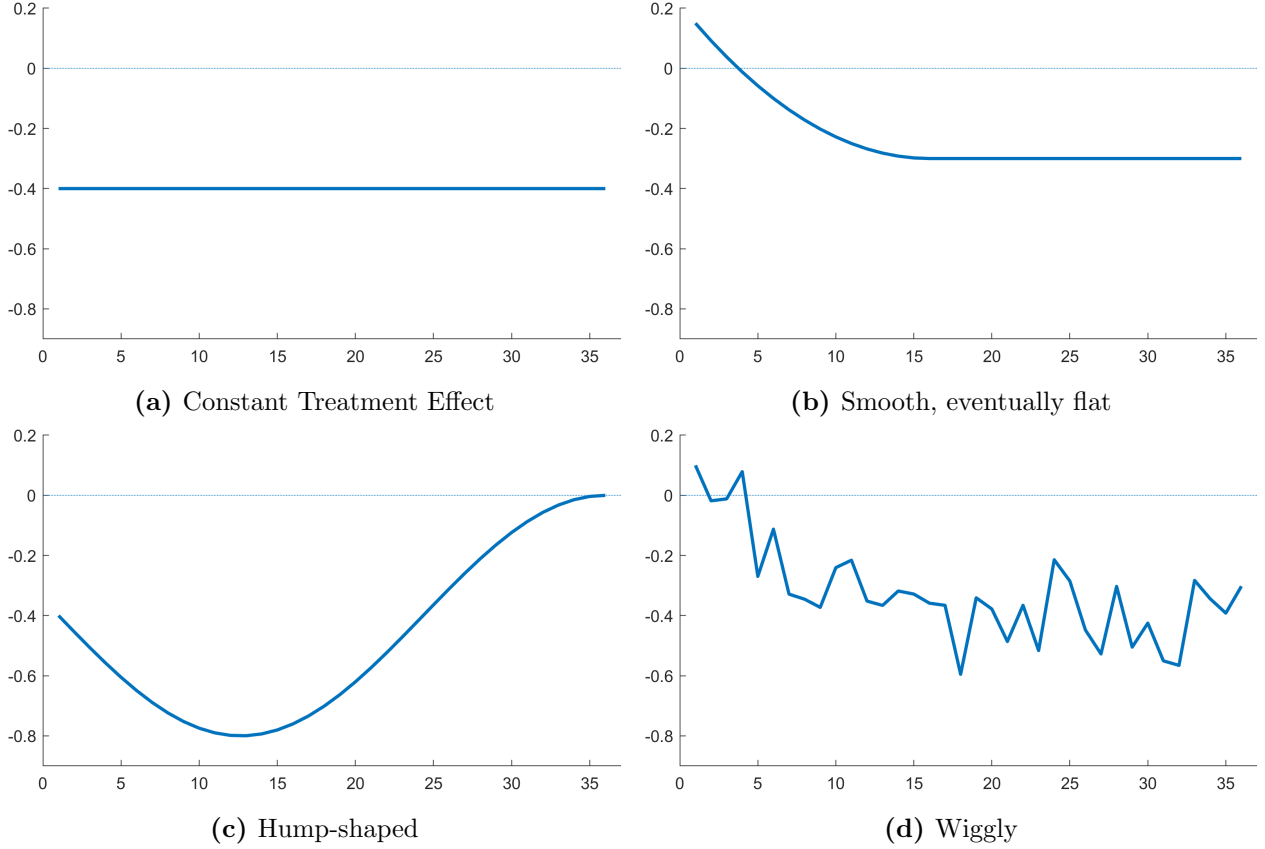


Figure 4: Four exemplary treatment effect paths β .

result is depicted in Figure 6, where we set $\alpha = 0.05$. The pointwise, sup-t, and restricted coverage numbers, as indicated by the three solid lines, represent the empirical analogue to the usual notion of uniform coverage for β : It reflects the fraction of simulations in which the true treatment path β falls entirely inside the pointwise confidence intervals (black), sup-t intervals (red), and restricted plausible bounds (yellow), respectively.

Across all four DGPs, the pointwise confidence intervals only cover the true treatment path in 15-20% of simulations. On the other hand, the sup-t intervals achieve nominal coverage across DGPs. The restricted plausible bounds are not constructed to provide uniform coverage for the true treatment path. It is thus not surprising that these bounds do not cover the entire treatment path in 95% of simulations across all DGPs. However, we do see that their coverage appears to converge towards 95% as the amount of noise in the initial estimates decreases (cf. Remark 2). Further, the restricted plausible bounds perform substantially better than the pointwise confidence intervals in covering the true treatment path when the true path is smooth. In the scenario of a wiggly treatment path, the restricted

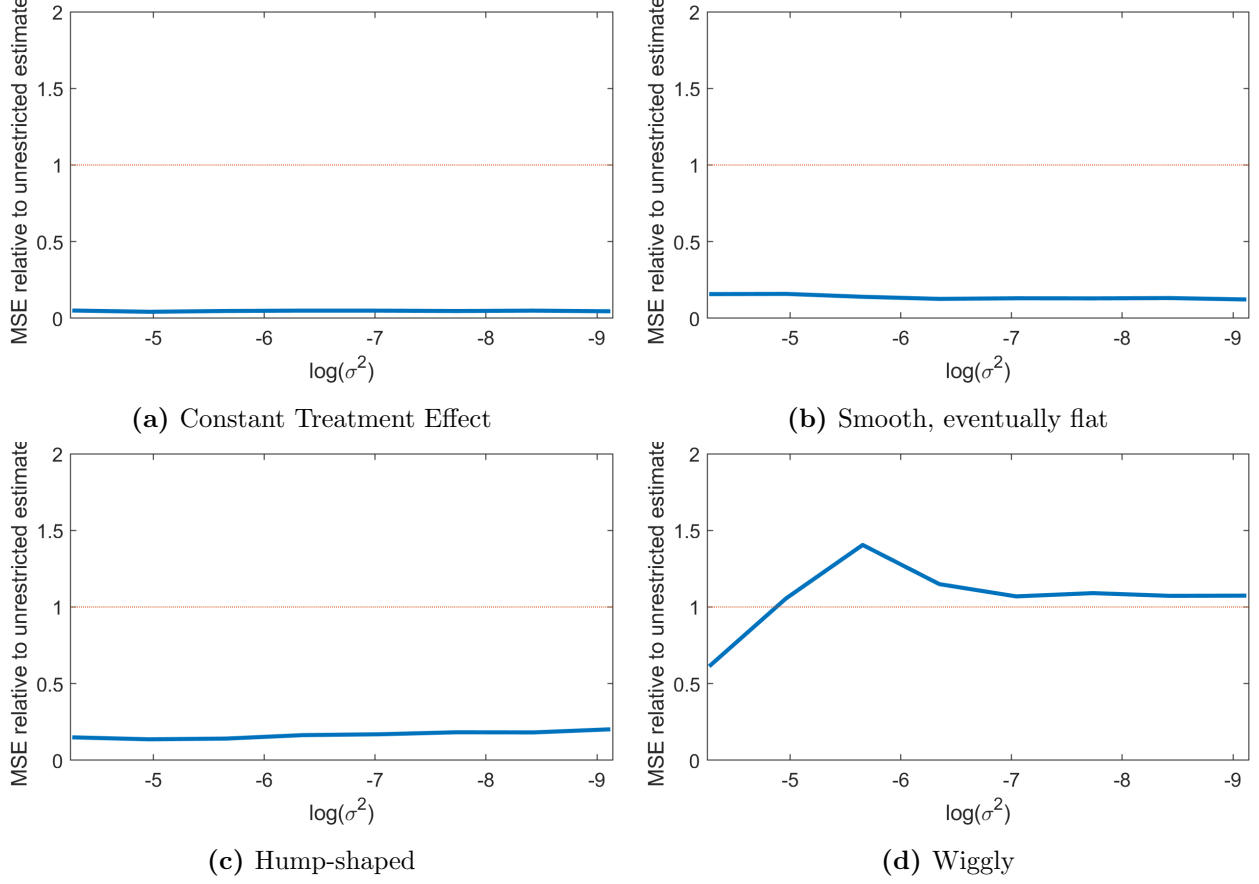


Figure 5: Relative performance of restricted and unrestricted estimators. Depicted is the ratio in mean-squared error between restricted and unrestricted estimates, $\frac{MSE(\tilde{\beta}(\hat{M}))}{MSE(\hat{\beta})}$, as a function of the amount of noise σ^2 in the initial estimates $\hat{\beta}$.

bounds exhibit poor coverage properties when the amount of noise in the initial estimates is large.

Proposition 2 guarantees that the plausible bounds cover the selected surrogate to the truth in at least 95% of realizations. In Figure 6, the restricted plausible bounds' coverage of the surrogate is illustrated by the dashed purple line. We see that this coverage is above 95% for all levels of σ^2 across all DGPs. We reemphasize that, in the scenario of a wiggly treatment path, a smooth approximation to the true path, for which we obtain valid coverage, may be a policy relevant object.

Finally, we note that, in line with Proposition 1, the cumulative bounds (as indicated by the dashed green lines) indeed cover the cumulative effect of the policy in 95% of simulations. That is, the true treatment path is on average within these bounds in 95% of simulations.

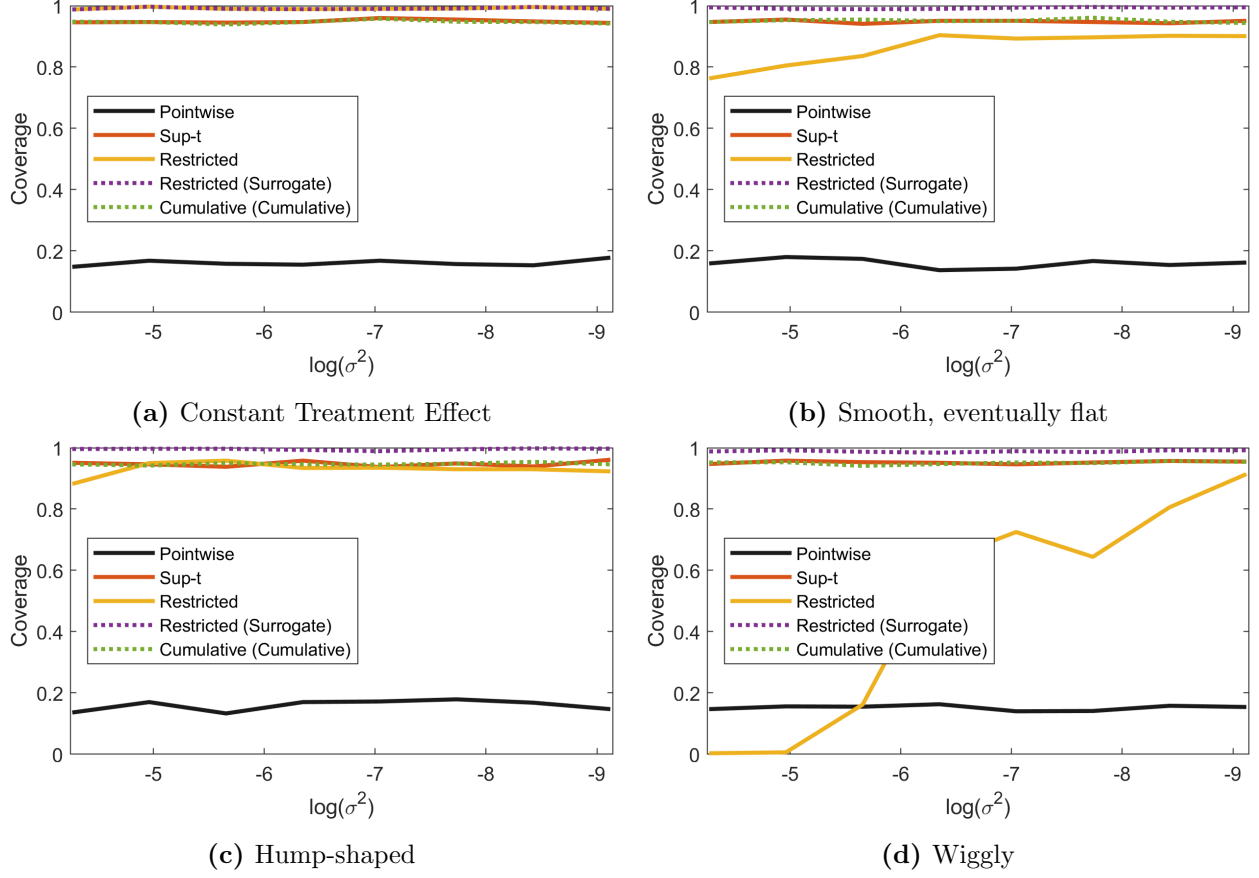


Figure 6: Coverage properties of various confidence regions as a function of the amount of noise σ^2 in the initial estimates $\hat{\beta}$.

In order to cover the true path in a higher fraction of simulations, the sup-t bands are generally wider than the pointwise bands (cf. Figure 2). We illustrate this across our simulations in Figure 7, which depicts the average width of the sup-t bands and the restricted bounds, relative to the pointwise intervals. While the sup-t bands are wider than the pointwise bands across the parameter space, the restricted bounds are in fact narrower throughout much of the parameter space, despite their improved coverage properties. For example, in the “Constant Treatment Effect” scenario, the restricted bounds are less than half as wide as the pointwise bands and less than a quarter as wide as the sup-t bands for all noise levels σ^2 . Yet, they cover close to 95% of all realizations, while the pointwise confidence intervals only cover the true treatment path in 15-20% of simulations.¹⁵ The

¹⁵As we show in Online Appendix Figure 13, we select surrogate paths β_M with significantly reduced degrees of freedom, relative to the unrestricted estimates, in the first three DPGs. This effective dimension reduction explains both the improvement in point estimation properties of $\tilde{\beta}(\hat{M})$ relative to the unrestricted estimates $\hat{\beta}$ documented in Figure 5, and the decrease in width of the confidence intervals documented in

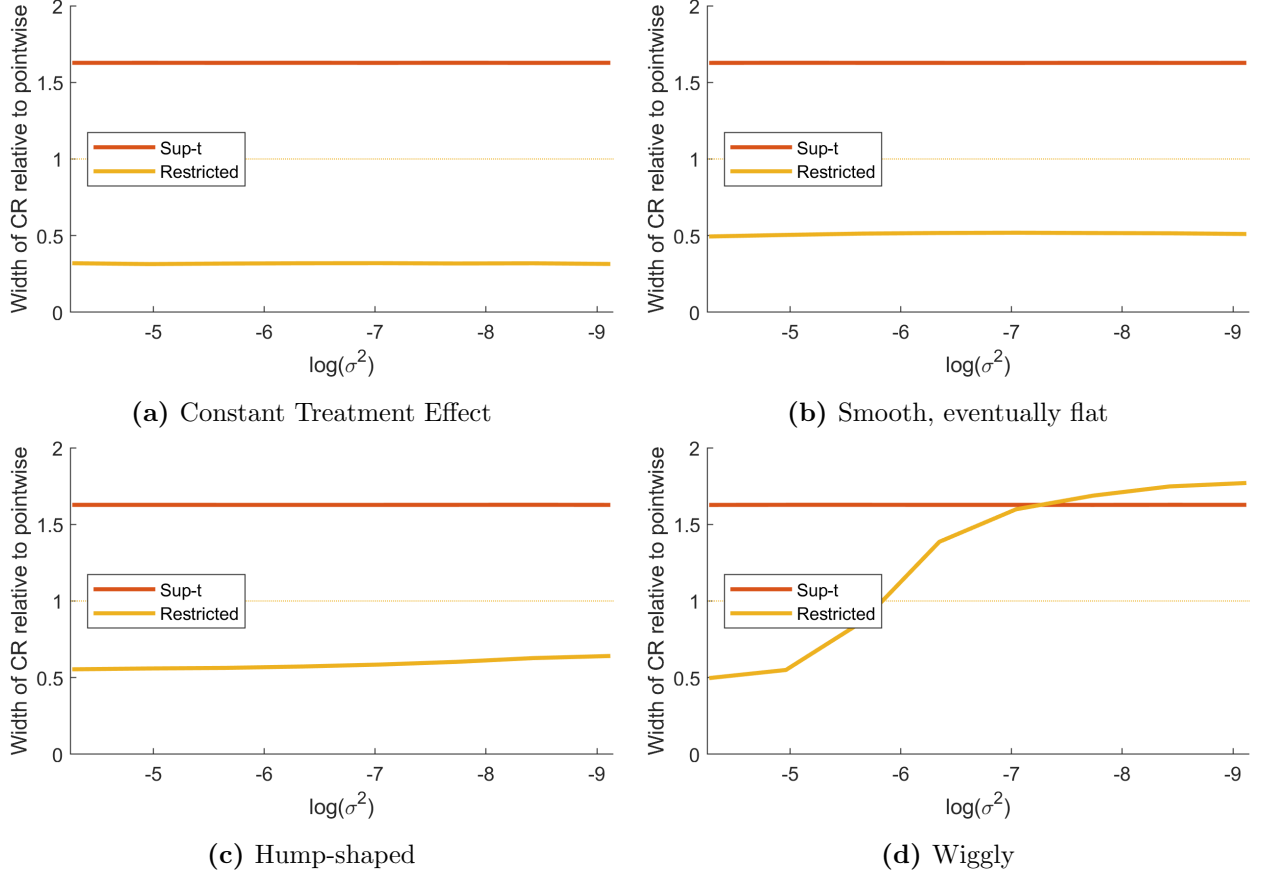


Figure 7: Average width of confidence regions relative to pointwise confidence intervals as a function of the amount of noise σ^2 in the initial estimates $\hat{\beta}$.

restricted bounds are only wider than the sup-t bands when (i) the treatment path is wiggly and (ii) there is very little noise. In this region of the parameter space, our model selection mechanism infers that the wiggles in the treatment path are large enough relative to the noise level that heavy smoothing will incur a large cost in terms of losing fit. With relatively little smoothing, our restricted plausible bounds are then slightly more conservative than the standard sup-t bands, which follows immediately from the results in Berk et al. [2013].

Finally, we shed some more light on the model selection of our procedure in Figure 8. Each panel depicts the 1,000 selected surrogates across our simulations in light brown. Since the chosen surrogates will depend on the precision of the initial estimates $\hat{\beta}$, we fix σ^2 at 0.014, corresponding to the amount of noise in the examples in Figure 3. When the true treatment path is smooth (Panels 8a-8c), the chosen surrogate tends to closely approximate the truth. In contrast, the chosen surrogate is often simpler than β while retaining its main

Figure 7.

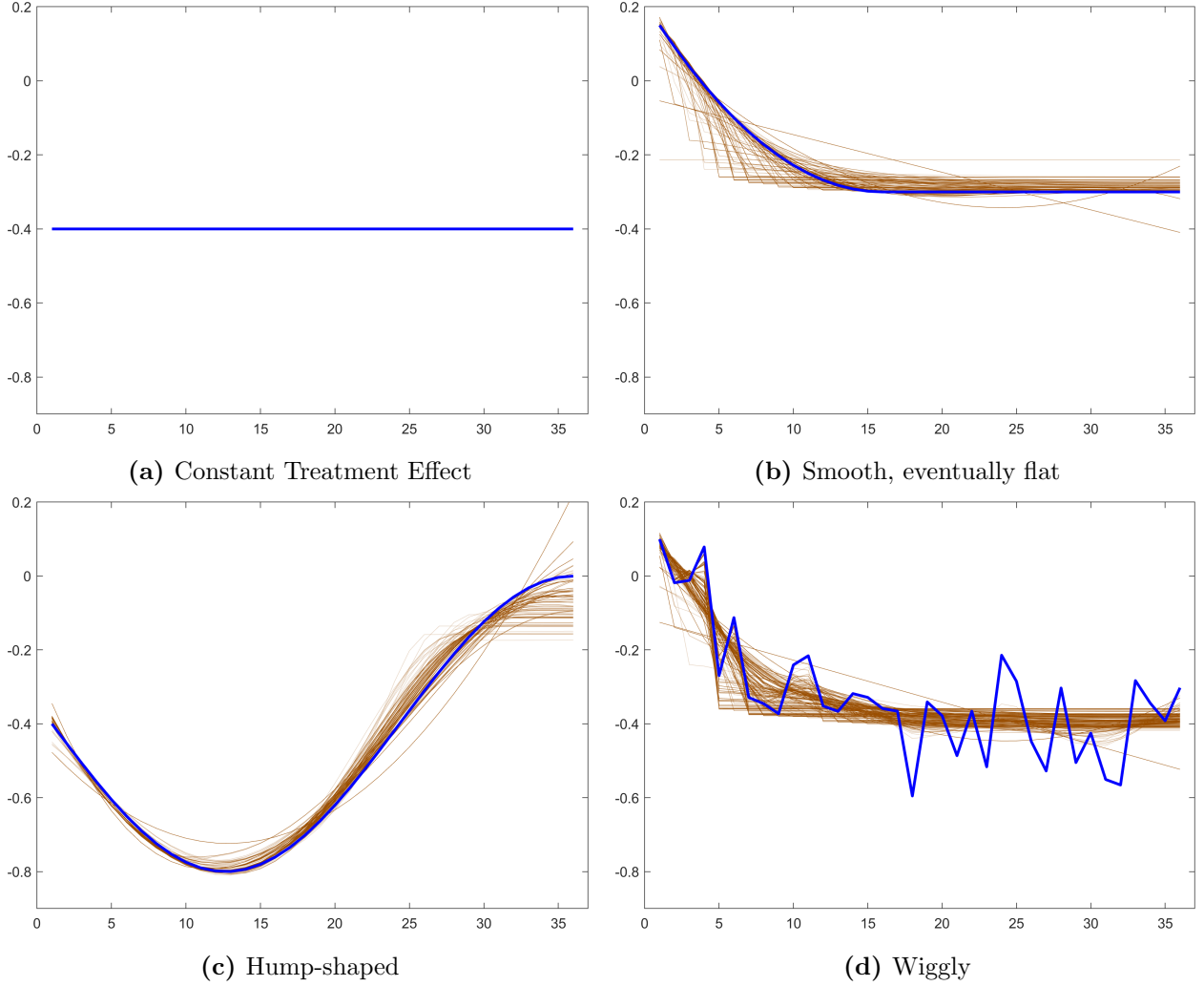


Figure 8: Illustration of the chosen surrogates across our 1,000 simulations for $\sigma^2 = 0.014$ ($\log(\sigma^2) = -4.27$), corresponding to the left most point in Figures 5-7, and thus a large amount of noise in $\hat{\beta}$.

features when the true treatment path is not smooth (Panel 8d).¹⁶

5 Conclusion

We are interested in (joint inference on) the dynamic treatment effect of a policy. We propose two visualization devices, which we term restricted and cumulative plausible bounds, to

¹⁶In Online Appendix Figure 14, we further illustrate how the chosen surrogates depend on σ^2 for our Wiggly DGP.

include in standard visualizations of estimated treatment effect paths. Because both bounds explicitly target objects other than uniformly covering the entire treatment path, they can be substantially tighter than standard pointwise and uniform confidence bands. Our bounds may thus provide useful insights about features of treatment effect paths when traditional confidence bands appear uninformative. Our bounds can also lead to markedly different conclusions relative to traditional visualizations when there is significant correlation in the estimates. As an auxiliary benefit, producing our restricted plausible bounds also provides additional restricted estimates that capture simplified representations of the dynamic effect path. Unsurprisingly, these restricted estimates have improved point estimation properties relative to the unrestricted estimates in settings where the treatment effect path is smooth.

It may be interesting to explore the notion of explicitly covering data-dependent surrogates in other economically relevant settings. While alternative model universes or model selection rules may be needed outside of the present setting, our proposal can easily be adapted to do so. For example, it would be interesting to explore related ideas in more structural settings.

References

- Shirley Almon. The distributed lag between capital appropriations and expenditures. *Econometrica*, pages 178–196, 1965.
- Timothy B Armstrong, Michal Kolesár, and Mikkel Plagborg-Møller. Robust empirical bayes confidence intervals. *Econometrica*, 90(6):2567–2602, 2022.
- Regis Barnichon and Christian Brownlees. Impulse response estimation by smooth local projections. *Review of Economics and Statistics*, 101(3):522–530, 2019.
- Regis Barnichon and Christian Matthes. Functional approximation of impulse responses. *Journal of Monetary Economics*, 99:41–55, 2018.
- Richard Berk, Lawrence Brown, Andreas Buja, Kai Zhang, and Linda Zhao. Valid post-selection inference. *The Annals of Statistics*, pages 802–837, 2013.
- Mariano Bosch and Raymundo M Campos-Vazquez. The trade-offs of welfare policies in labor markets with informal jobs: The case of the “seguro popular” program in Mexico. *American Economic Journal: Economic Policy*, 6(4):71–99, 2014.

- Levi Boxell, Matthew Gentzkow, and Jesse M. Shapiro. Cross-country trends in affective polarization. *The Review of Economics and Statistics*, 106(2):557–565, 2024.
- Brantly Callaway and Pedro H.C. Sant’Anna. Difference-in-differences with multiple time periods. *Journal of Econometrics*, 225(2):200–230, 2021.
- Xiaohong Chen, Timothy Christensen, and Sid Kankanala. Adaptive estimation and uniform confidence bands for nonparametric structural functions and elasticities. *The Review of Economic Studies*, forthcoming.
- Joachim Freyberger and Yoshiyasu Rai. Uniform confidence bands: Characterization and optimality. *Journal of Econometrics*, 204(1):119–130, 2018.
- Joachim Freyberger and Brandon Reeves. Inference under shape restrictions. *Available at SSRN 3011474*, 2018.
- Christopher Genovese and Larry Wasserman. Adaptive confidence bands. *The Annals of Statistics*, pages 875–905, 2008.
- Atsushi Inoue and Lutz Kilian. Joint confidence sets for structural impulse responses. *Journal of Econometrics*, 192(2):421–432, 2016.
- Òscar Jordà. Simultaneous confidence regions for impulse responses. *The Review of Economics and Statistics*, 91(3):629–647, 2009.
- Òscar Jordà. Local projections for applied economics. *Annual Review of Economics*, 15(1):607–631, 2023.
- Arun K Kuchibhotla, John E Kolassa, and Todd A Kuffner. Post-selection inference. *Annual Review of Statistics and Its Application*, 9(1):505–527, 2022.
- Hannes Leeb and Benedikt M. Pötscher. Model selection and inference: Facts and fiction. *Econometric Theory*, 21(1):21–59, 2005.
- Dake Li, Mikkel Plagborg-Møller, and Christian K Wolf. Local projections vs. vars: Lessons from thousands of dgps. *Journal of Econometrics*, page 105722, 2024.
- Emi Nakamura and Jón Steinsson. Identification in macroeconomics. *Journal of Economic Perspectives*, 32(3):59–86, 2018.

- José Luis Montiel Olea and Mikkel Plagborg-Møller. Simultaneous confidence bands: Theory, implementation, and an application to SVARs. *Journal of Applied Econometrics*, 34(1): 1–17, 2019.
- José Luis Montiel Olea, Mikkel Plagborg-Møller, Eric Qian, and Christian K Wolf. Double robustness of local projections and some unpleasant varithmetic. Technical report, National Bureau of Economic Research, 2024.
- Mikkel Plagborg-Møller. *Essays in macroeconometrics*. PhD thesis, 2016.
- Jonathan Roth. Pretest with caution: Event-study estimates after testing for parallel trends. *American Economic Review: Insights*, 4(3):305–322, 2022.
- Robert J Shiller. A distributed lag estimator derived from smoothness priors. *Econometrica*, pages 775–788, 1973.
- Christopher A Sims and Tao Zha. Error bands for impulse responses. *Econometrica*, 67(5): 1113–1155, 1999.
- Jonathan Taylor and Robert J Tibshirani. Statistical learning and selective inference. *Proceedings of the National Academy of Sciences*, 112(25):7629–7634, 2015.

Online Appendix

A A primer on confidence regions

If β is a scalar, the standard approach in economics to quantify and visualize the uncertainty associated with an estimate for β is to construct a confidence interval. For a chosen size α , such a confidence interval covers the true value β in $100 * (1 - \alpha)\%$ of all realizations of the data: $\mathbb{P}(\ell(X) < \beta < u(X)) = 1 - \alpha$ where $\ell(X)$ and $u(X)$ denote the lower and upper bounds of the confidence interval and observed data are a realization from random variable X . Intuitively, these intervals visualize to the reader what values of β are “plausible” based on the observed data. The idea being that values inside this confidence interval appear “plausible,” while values outside of the interval do not. More formally, values outside this interval are rejected by a standard t-test at level α , while values inside the interval are not rejected.

Since in this paper a dynamic treatment path is the object of interest, $\beta = \{\beta_h\}_{h=1}^H$ is an ordered vector instead. We start with a diagram in Online Appendix Figure 9 that illustrates standard methods in the case of a two dimensional parameter $\beta = (\beta_1, \beta_2)$ where estimates are $\hat{\beta} = (\hat{\beta}_1, \hat{\beta}_2) = (2, 1)$ and $V_\beta = I_2$ is the 2×2 identity matrix.

The predominant practice today is to include pointwise confidence intervals in depictions of estimated treatment effect paths. $100 * (1 - \alpha)\%$ pointwise intervals for a specific β_h simply correspond to choosing $(\ell_h(X), u_h(X)) = (\hat{\beta}_h - z_{1-\alpha/2} \sqrt{V_\beta[h, h]}, \hat{\beta}_h + z_{1-\alpha/2} \sqrt{V_\beta[h, h]})$ where $V_\beta[h, h]$ is the variance of $\hat{\beta}_h$ and $z_{1-\alpha/2}$ is the $1 - \alpha/2$ quantile of a standard normal distribution. For example, the pointwise 95% confidence intervals in the case of the example in Online Appendix Figure 9 for β_1 and β_2 are respectively 2 ± 1.96 and 1 ± 1.96 . Correspondingly, the black square depicts the Cartesian product of these pointwise confidence intervals for β_1 and β_2 . Denote the region provided by the black square as CR^{pw} . Treated as a confidence region for (β_1, β_2) , CR^{pw} ignores any information in the off-diagonal entries in the covariance matrix of $\hat{\beta}$ and b) is only valid for testing pre-specified hypotheses involving single coefficients. Thus, it does not achieve correct coverage for the vector $\beta = (\beta_1, \beta_2)$: For a chosen significance level α , it will generally be true that $\mathbb{P}(\beta \in CR^{pw}) = \mathbb{P}(\ell_h(X) < \beta_h < u_h(X) \forall h) < (1 - \alpha)$, such that the black square will generally cover the true parameter β in less than $100(1 - \alpha)\%$ of realizations of the data. For example, if $Cov(\hat{\beta}_1, \hat{\beta}_2) = 0$, the probability that the pointwise confidence region covers

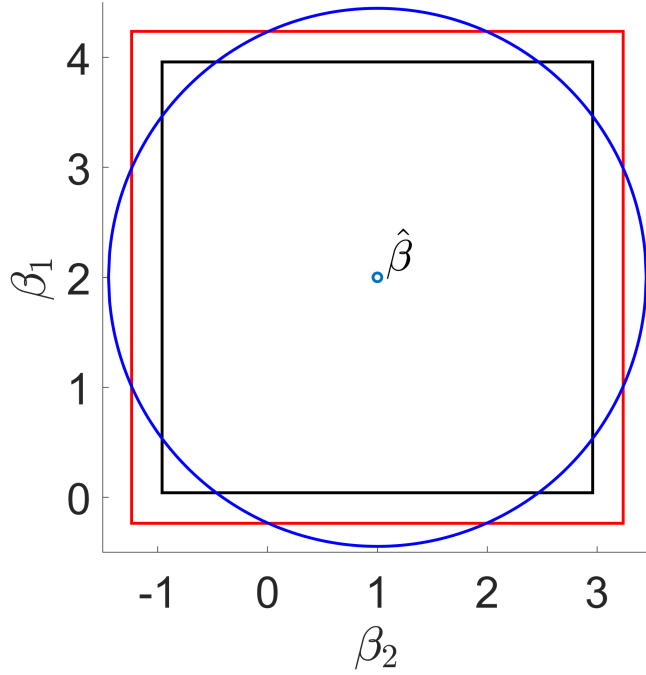
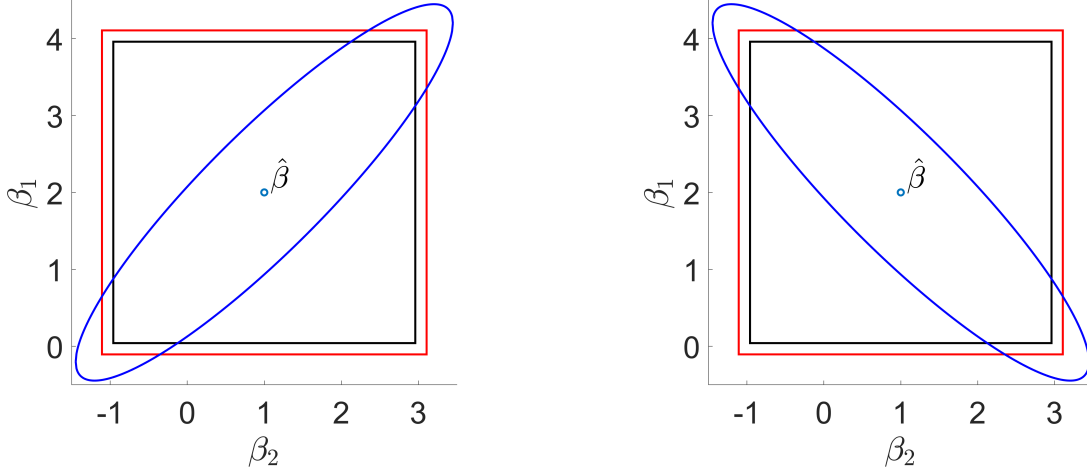


Figure 9: Illustration of different confidence regions. Pointwise (black), sup-t (red), and Wald (blue) 95% confidence region in two dimensions. $\hat{\beta} = (2, 1)$ with covariance matrix $V_{\beta} = I_2$.

the vector β will be $P(\beta \in CR^{pw}) = (1 - \alpha)^2$.

One way to construct a uniformly valid confidence region is to take the Cartesian product of sup-t confidence intervals (depicted in red) instead. Denote this region CR^{sup-t} . Sup-t intervals are easy to construct, and simply use a slightly large critical value compared to pointwise confidence intervals. Specifically, $100(1 - \alpha)\%$ sup-t intervals are constructed by choosing $(\ell_h(X), u_h(X)) = (\hat{\beta}_h - c_{\alpha}\sqrt{V_{\beta}[h, h]}, \hat{\beta}_h + c_{\alpha}\sqrt{V_{\beta}[h, h]})$ where c_{α} is set such that $\mathbb{P}(\ell_h(X) < \beta_h < u_h(X) \forall h) \geq (1 - \alpha)$. For a chosen significance level α , CR^{sup-t} thus achieves valid coverage, since $\mathbb{P}(\beta \in CR^{sup-t}) \geq (1 - \alpha)$ by construction. For example, the sup-t 95% confidence intervals in the case of the example in Online Appendix Figure 9 for β_1 and β_2 are respectively 2 ± 2.24 and 1 ± 2.24 . See, e.g., Freyberger and Rai [2018] and Olea and Plagborg-Møller [2019] for details about sup-t interval construction as well as further discussion of different (rectangular) confidence regions. We focus on pointwise and sup-t confidence intervals, since these two are the predominant intervals used in practice (e.g. Callaway and Sant’Anna [2021]; Jordà [2023]; Boxell et al. [2024]).

Finally, the blue circle in Online Appendix Figure 9 corresponds to an alternative confidence region for β , namely the Wald confidence region. Denote this region CR^{Wald} . This



(a) Positive correlation ($Cov(\beta_1, \beta_2) = 0.9$).

(b) Negative correlation ($Cov(\beta_1, \beta_2) = -0.9$).

Figure 10: Illustration of different confidence regions with non-zero correlation. Pointwise (black), Sup-t (red), and Wald (blue) 95% confidence region in two dimensions. $\hat{\beta} = (2, 1)$. $Var(\beta_1) = Var(\beta_2) = 1$.

region simply collects all parameter values (b_1, b_2) that are not rejected by a standard Wald test of the null hypothesis that $(\beta_1, \beta_2) = (b_1, b_2)$ at level α . For a chosen significance level α , this region also achieves valid coverage: $\mathbb{P}(\beta \in CR^{Wald}) = (1 - \alpha)$ by construction.

Online Appendix Figure 10 illustrates the three considered confidence regions in settings with non-zero correlation between the two estimates. We first note that the pointwise confidence region is identical in Online Appendix Figures 9 and 10, reflecting the fact that this region does not depend on the off-diagonal entries in $Var(\hat{\beta})$. Second, while the sup-t region does depend on the off-diagonal entries in $Var(\hat{\beta})$, it only does so in a limited way through the critical value c_α . In this example, the sup-t region is different between Online Appendix Figures 9 and 10, but identical in Online Appendix Figures 10a and 10b. In contrast, the Wald confidence region differs meaningfully in all three figures. This illustration suggests that the off-diagonal entries in V_β can have important implications for the construction of confidence regions, but that traditional event study plots may be ineffective at visualizing these implications.

B Algorithmic implementation

Recall that the algorithm takes as input jointly normal estimates of the treatment path $\hat{\beta} \sim N(\beta, V_\beta)$, where $V_\beta = \sigma^2 V$, $\sigma^2 = \frac{1}{H} \sum_{h=1}^H V_\beta(h, h)$, and V is positive-definite. We define the following object:

$$\begin{aligned} \tilde{\beta}(\lambda_1, \lambda_2, K) &= \arg \min_b Q(b, \lambda_1, \lambda_2, K) \\ &= \arg \min_b \underbrace{(\hat{\beta} - b)' V^{-1} (\hat{\beta} - b)}_{\text{distance from } \hat{\beta}} + \lambda_1 \underbrace{b' D_1' W_1(K) D_1 b}_{\text{penalty on first difference after horizon } K} + \lambda_2 \underbrace{b' D_3' W_3 D_3 b}_{\text{penalty on third difference}}, \end{aligned}$$

where

- λ_1, λ_2, K are tuning parameters that determine the surrogate M
- D_1 and D_3 are the $H \times (H - 1)$ and $H \times (H - 3)$ first and third difference operators
- $V_1 = D_1 V D_1'$, $V_3 = D_3 V D_3'$ are (scaled) variance matrices for first and third differences
- $V_1(K)$ is the $(H - K) \times (H - K)$ matrix consisting of the lower right entries of V_1 , $V_1(K : H - 1, K : H - 1)$
- $\bar{V}_3 = \frac{1}{H-3} \sum_{h=1}^{H-3} V_3(h, h)$, $\bar{V}_1(K) = \frac{1}{H-K} \sum_{h=K}^{H-1} V_1(h, h)$
- $W_1(K) = \begin{pmatrix} \mathbf{0}_{(K-1) \times (K-1)} & \mathbf{0}_{(K-1) \times (H-K)} \\ \mathbf{0}_{(H-K) \times (K-1)} & \text{diag}(V_1(K)) / \bar{V}_1(K) \end{pmatrix}$
- $W_3 = \text{diag}(V_3) / \bar{V}_3$

Intuitively, $W_1(K)$ and W_3 are analogs to natural scaling in standard ridge with independent columns but different variances.

To select the surrogate M from the data we choose $M = (\lambda_1, \lambda_2, K)$ that minimizes a BIC analog over \mathcal{M} : $\hat{M} = \arg \min_{M \in \mathcal{M}} (\hat{\beta} - \tilde{\beta}(M))' V_\beta^{-1} (\hat{\beta} - \tilde{\beta}(M)) + \log(H) \text{df}(\lambda_1, \lambda_2, K)$. The universe of models considered, \mathcal{M} , includes

- (a) A constant, linear, quadratic, and cubic treatment effect model (with one, two, three, and four degrees of freedom respectively)
- (b) Surrogates of the form $P(M)\beta = \beta(\lambda_1, \lambda_2, K)$ using a grid over $(\lambda_1, \lambda_2, K)$

(c) the unrestricted estimates $\hat{\beta}$ ($df = H$)

We construct the grid for the surrogates under (b) as follows. First, we set lower and upper bounds for λ_1 and λ_2 . Independent of K , these bounds are equal to $(\underline{\lambda}_1, \bar{\lambda}_1) = (e^{-10}, e^{10})$, and $(\underline{\lambda}_2, \bar{\lambda}_2) = (e^{-10}, \bar{\lambda}_2)$, where $\bar{\lambda}_2$ is defined as the λ_2 such that $df(e^{-10}, \lambda_2, K) = 4$.¹⁷ Note that, with $\lambda_1 = 0$, $\bar{\lambda}_2$ also does not depend on K . We then consider the Cartesian product of an equal spaced grid of 20 points between $(\log(\underline{\lambda}_1), \log(\bar{\lambda}_1))$ and equal spaced grid of 20 points between $(\log(\underline{\lambda}_2), \log(\bar{\lambda}_2))$, and retain those grid points with $df \in [4, H - 1]$.

¹⁷Recall that $df(\lambda_1, \lambda_2, K) = \text{trace} \left((V^{-1} + \lambda_1 D'_1 W_1(K) D_1 + \lambda_2 D'_3 W_3 D_3)^{-1} V^{-1} \right)$.

C Simulation design

Scenario	treatment path β
Constant treatment effect	$\beta_h = -0.4 \forall h$
Smooth, eventually flat	$\beta_h = \begin{cases} -0.289 + \frac{(18-h)^2}{1000} & h \leq 17 \\ -0.289 & h \geq 18 \end{cases}$
Hump-shaped	$\beta_h = -0.4 - 0.4 \sin\left(\frac{3}{70}\pi(h-1)\right) \forall h$
Wiggly	$\beta_h = \check{\beta}_h + \xi_h, \text{ where } \xi_h \sim N(0, 0.1) \text{ iid across } h \text{ and}$ $\check{\beta}_h = \begin{cases} -0.4 \sin\left(\frac{1}{35}\pi(h-1)\right) & h \leq 19 \\ -0.4 & h \geq 20 \end{cases}$

Table 1: Detailed description of the four different treatment paths $\beta = \{\beta\}_{h=1}^{36}$ considered in the simulations. We draw a single realization of the “Wiggly” scenario (which is depicted in Figure 4d) to use throughout our simulations.

We generate the covariance matrix of $\hat{\beta}$ as $V_{\beta} = \sigma^2 * \text{diag}(S)R \text{diag}(S)$, where $S_h = (100 + h)/100$, and R is a $H \times H$ Toeplitz matrix with $R_{ij} = \rho^{|i-j|}$. For all results in the main text, we set $\rho = 0$ (such that R becomes the identity matrix).

D Additional simulation results

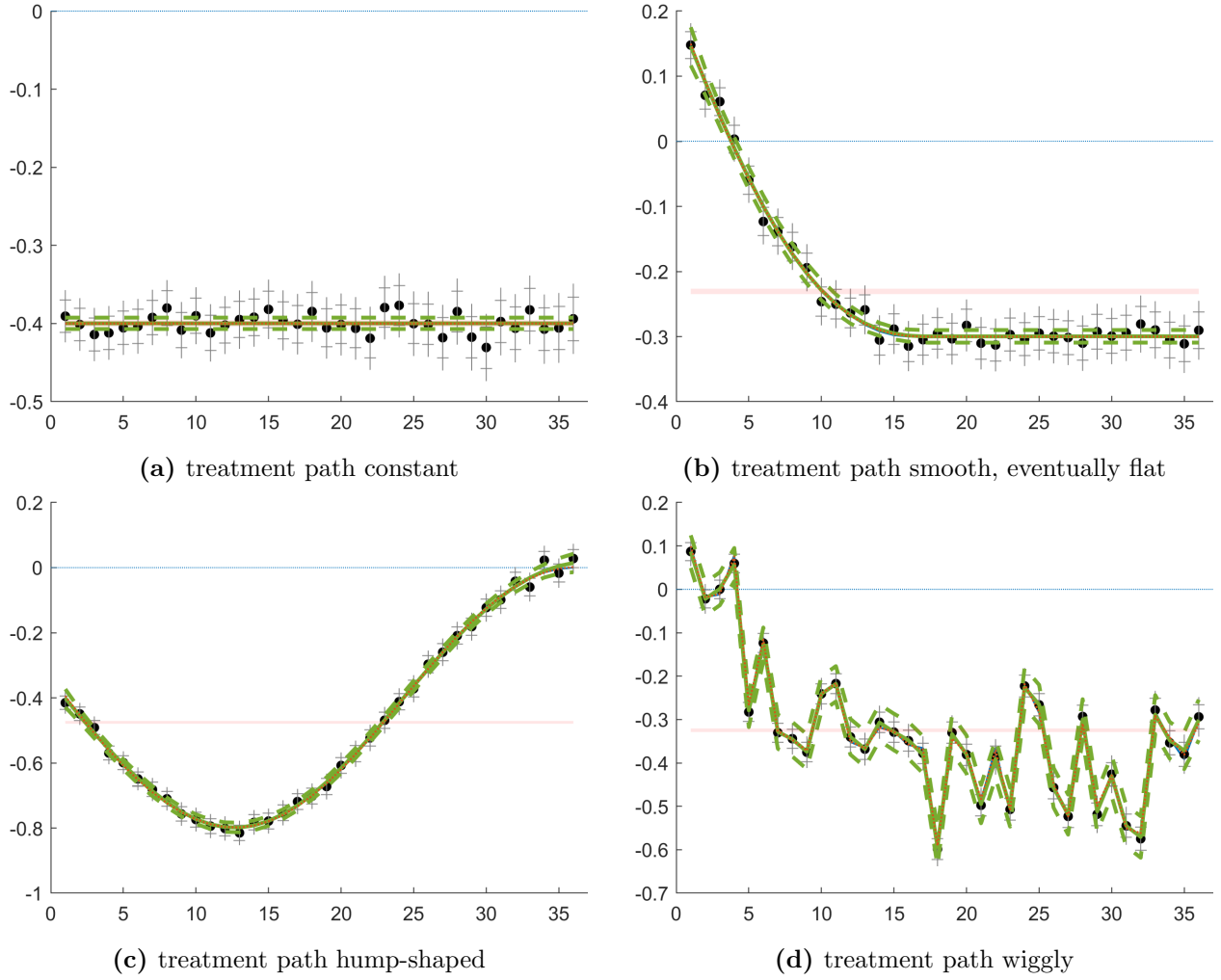
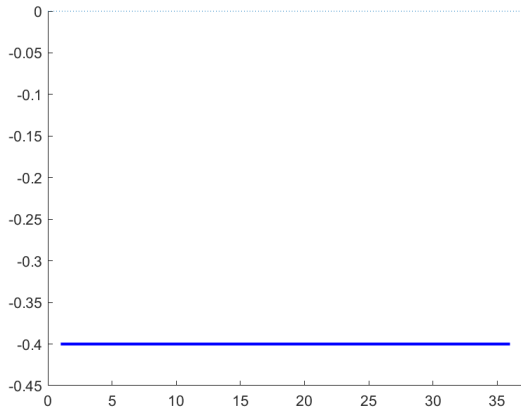
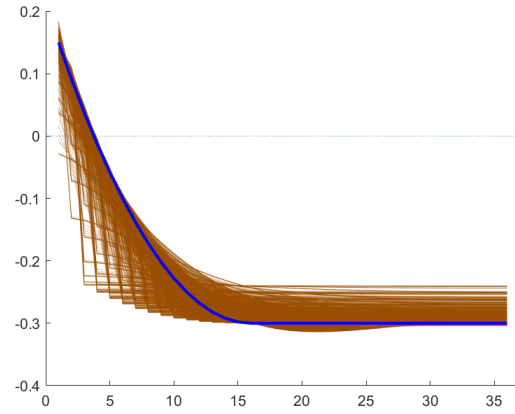


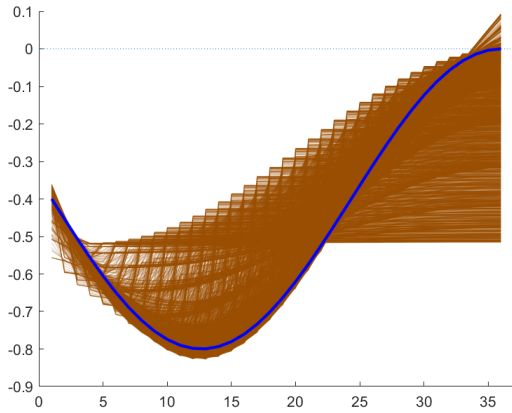
Figure 11: Exemplary event-study plots including our proposals with smaller noise than in Figure 3.



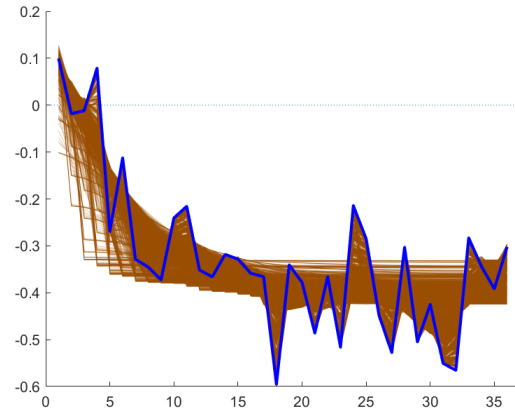
(a) Constant Treatment Effect



(b) Smooth, eventually flat



(c) Hump-shaped



(d) Wiggly

Figure 12: Illustration of Model universe \mathcal{M} . Brown lines correspond to all considered models M of the form $P(M)\beta = \beta(\lambda_1, \lambda_2, K)$ with $df \in [4, H - 1]$. Blue line corresponds to true treatment effect β .

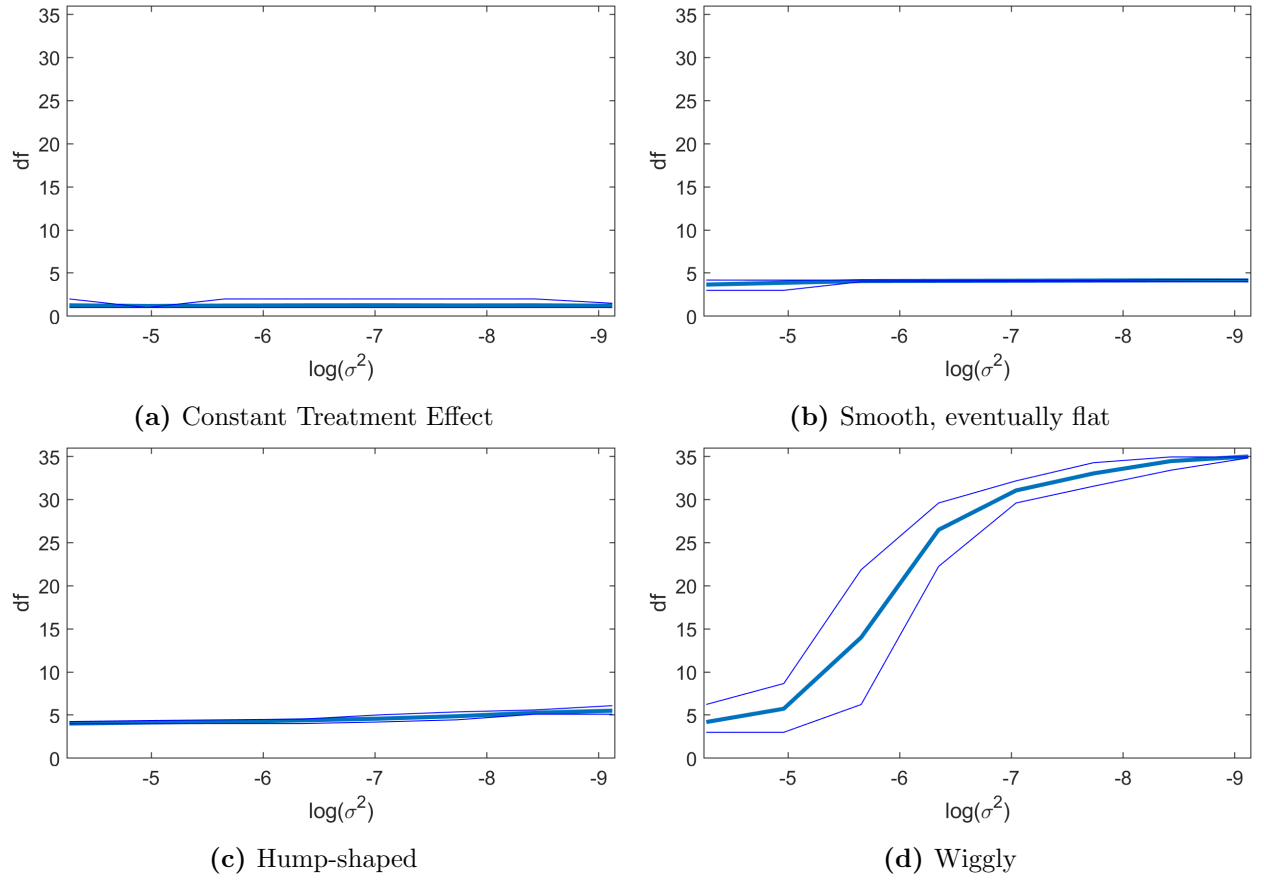
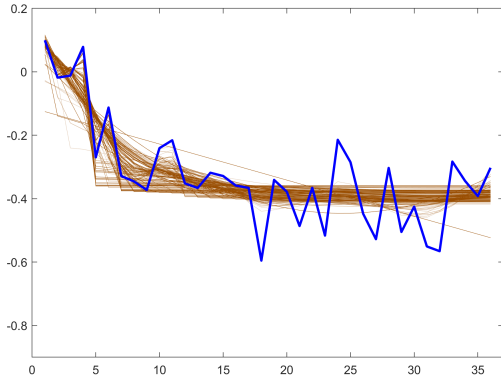
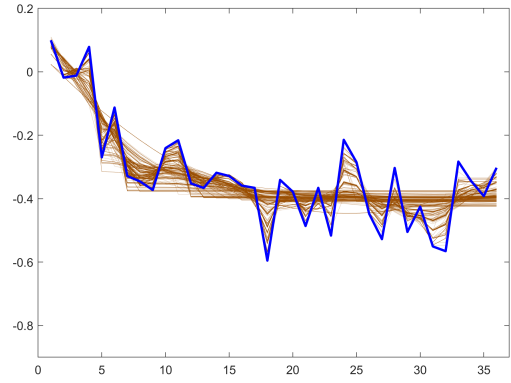


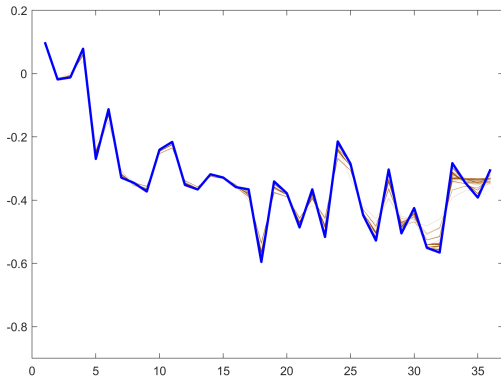
Figure 13: Chosen df across realizations for restricted estimates as a function of the amount of noise σ^2 in the initial estimates $\hat{\beta}$.



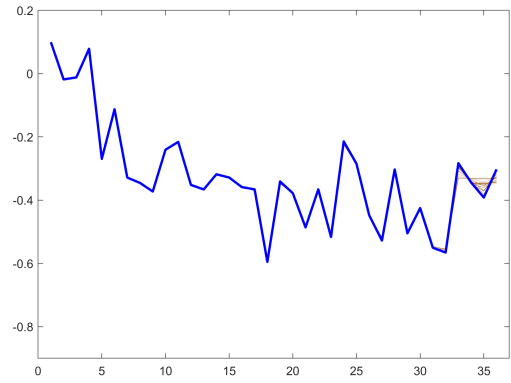
(a) $\log(\sigma^2) = -4.27$



(b) $\log(\sigma^2) = -5.66$



(c) $\log(\sigma^2) = -7.04$



(d) $\log(\sigma^2) = -8.43$

Figure 14: Illustration of 1,000 chosen surrogates for Wiggly DGP for various levels of σ^2 , the amount of noise in the initial estimates $\hat{\beta}$.

E Simulation results with positively correlated estimates

In this appendix, we repeat the simulation experiment reported in the main test using a covariance matrix V_β capturing positively correlated estimates. In particular, recall that $V_\beta = \sigma^2 * \text{diag}(S)R \text{diag}(S)$, where $S_h = (100 + h)/100$, and R is a $H \times H$ Toeplitz matrix with $R_{ij} = \rho^{|i-j|}$. In the results that follow, we set $\rho = 0.8$.

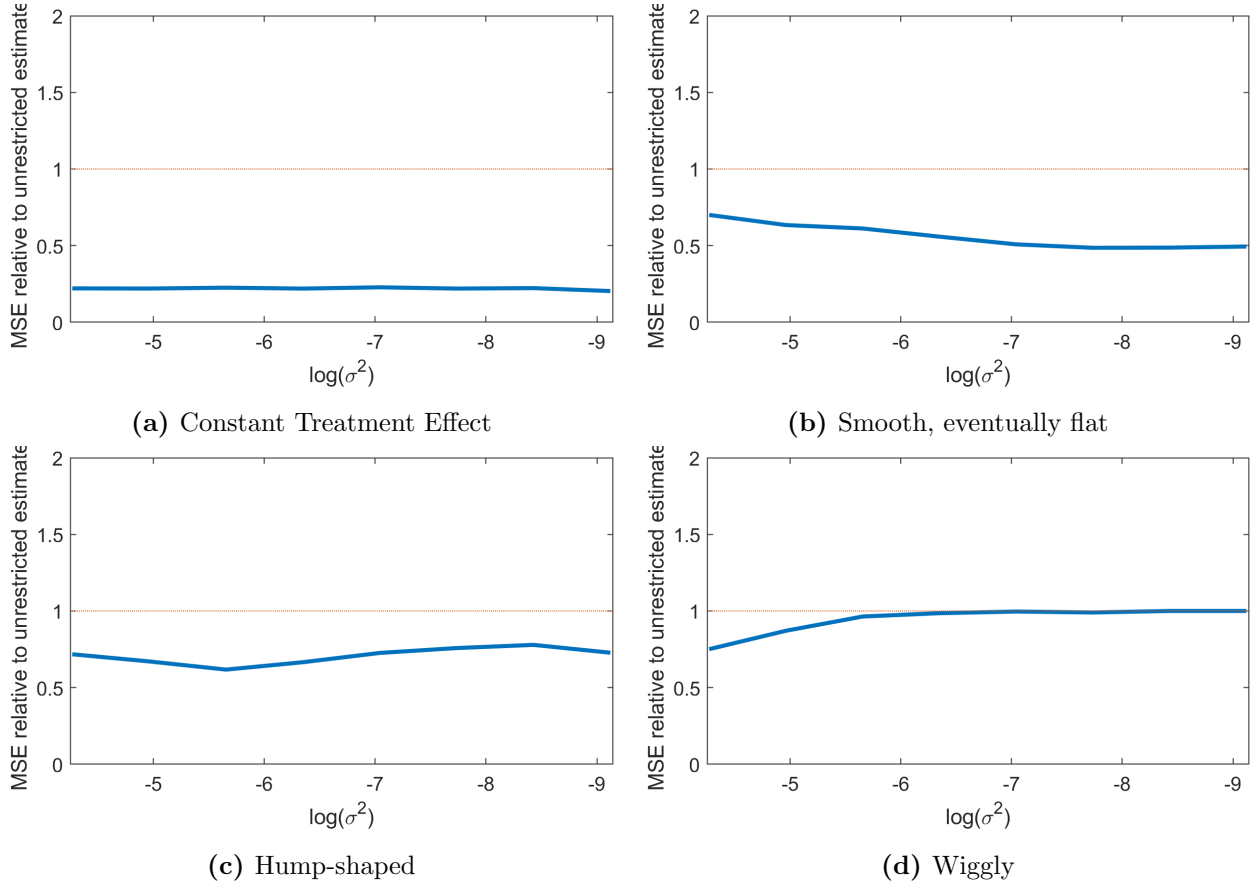
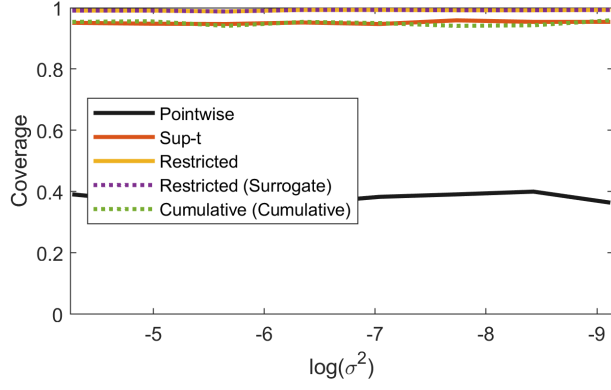
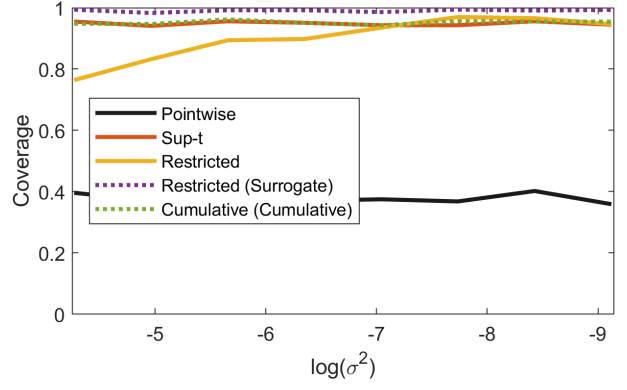


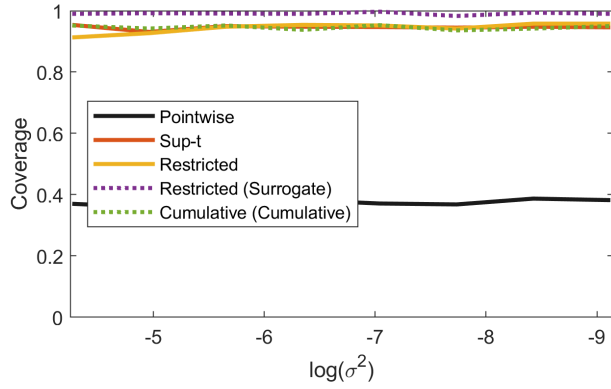
Figure 15: Relative performance of restricted and unrestricted estimators. Depicted is the ratio $\frac{MSE(\tilde{\beta}(\hat{M}))}{MSE(\hat{\beta})}$ as a function of the amount of noise in the initial estimates $\hat{\beta}$.



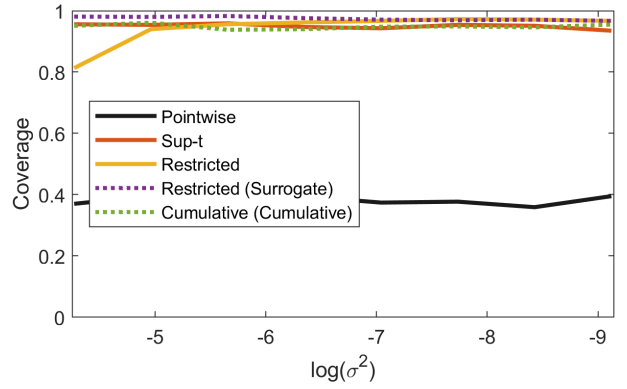
(a) Constant Treatment Effect



(b) Smooth, eventually flat



(c) Hump-shaped



(d) Wiggly

Figure 16: Coverage properties of various confidence regions as a function of the amount of noise in the initial estimates $\hat{\beta}$.

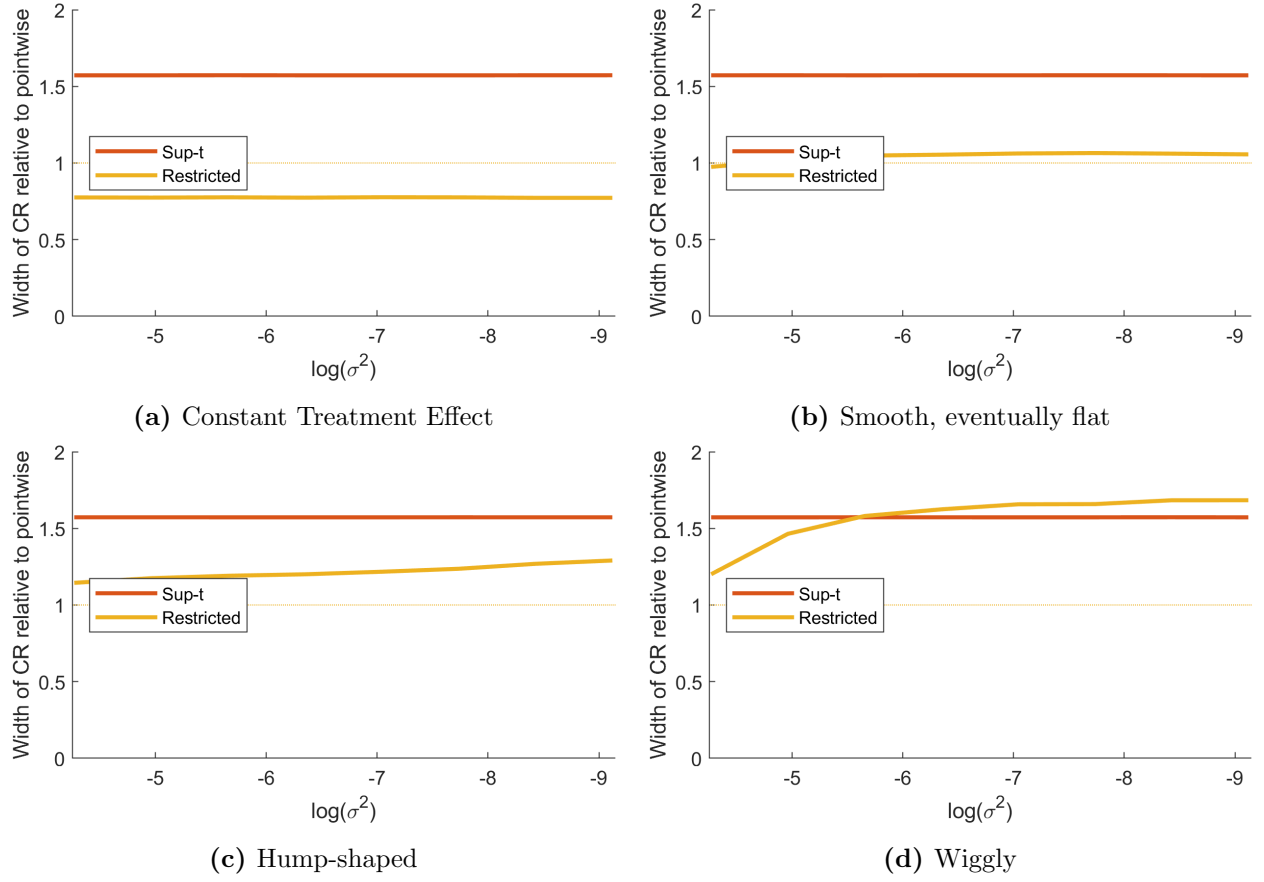


Figure 17: Average width of confidence regions relative to pointwise confidence intervals as a function of the amount of noise in the initial estimates $\hat{\beta}$.

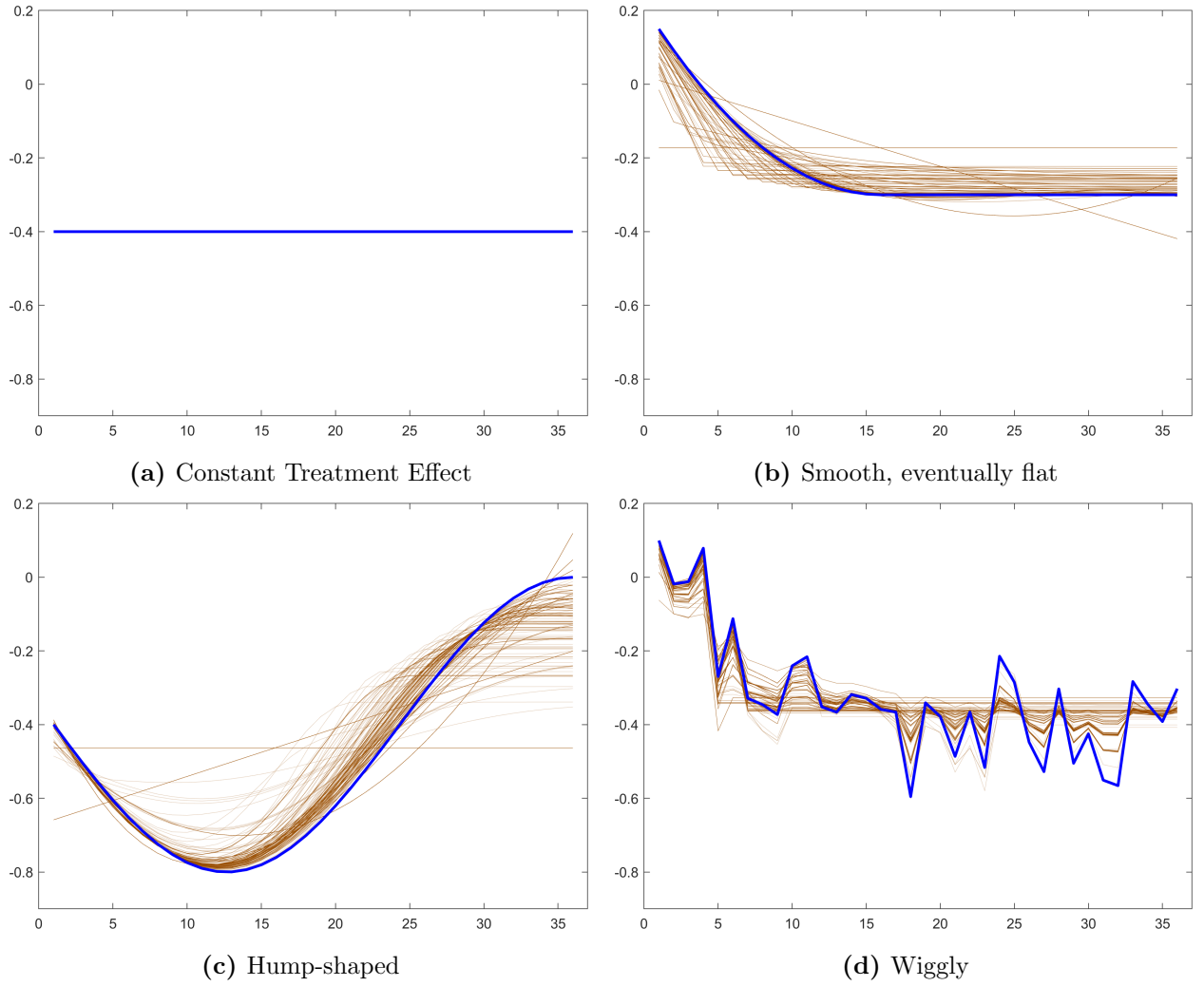


Figure 18: Illustration of the 1,000 chosen surrogates for $\sigma^2 = 0.014$ ($\log(\sigma^2) = -4.27$) under positive correlation in the point estimates.